

# **Central Lancashire Online Knowledge (CLoK)**

Title	Crafting y-L-Glutamyl-l-Cysteine layered Human Serum Albumin- nanoconstructs for brain targeted delivery of ropinirole to attenuate cerebral ischemia/reperfusion injury via "3A approach"				
Туре	Article				
URL	https://clok.uclan.ac.uk/id/eprint/44194/				
DOI	https://doi.org/10.1016/j.biomaterials.2022.121805				
Date	2022				
Citation	Fatima, Saman, Ali, Mubashshir, Quadri, Syed Naved, Beg, Sarwar, Samim, M, Parvez, Suhel, Abdin, Malik Zainul, Mishra, Prashant and Ahmad, Farhan Jalees (2022) Crafting γ-L-Glutamyl-l-Cysteine layered Human Serum Albumin-nanoconstructs for brain targeted delivery of ropinirole to attenuate cerebral ischemia/reperfusion injury via "3A approach". Biomaterials, 289. p. 121805. ISSN 1878-5905				
Creators	Fatima, Saman, Ali, Mubashshir, Quadri, Syed Naved, Beg, Sarwar, Samim, M, Parvez, Suhel, Abdin, Malik Zainul, Mishra, Prashant and Ahmad, Farhan Jalees				

It is advisable to refer to the publisher's version if you intend to cite from the work. https://doi.org/10.1016/j.biomaterials.2022.121805

For information about Research at UCLan please go to <a href="http://www.uclan.ac.uk/research/">http://www.uclan.ac.uk/research/</a>

All outputs in CLoK are protected by Intellectual Property Rights law, including Copyright law. Copyright, IPR and Moral Rights for the works on this site are retained by the individual authors and/or other copyright owners. Terms and conditions for use of this material are defined in the http://clok.uclan.ac.uk/policies/

Crafting γ-L-Glutamyl-L-Cysteine Layered Human Serum Albumin-Nanoconstructs for Brain Targeted Delivery of Ropinirole to Attenuate Cerebral Ischemia/Reperfusion Injury via "3A Approach"

Saman Fatima<sup>a</sup>, Mubashshir Ali<sup>b</sup>, Syed Naved Quadri<sup>c</sup>, Sarwar Beg<sup>d</sup>, M. Samim<sup>e</sup>, Suhel Parvez<sup>b</sup>, Malik Zainul Abdin<sup>c</sup>, Prashant Mishra<sup>f</sup> and Farhan Jalees Ahmad<sup>a,\*</sup>

<sup>a</sup>Department of Pharmaceutics, School of Pharmaceutical Education and Research (SPER), Jamia Hamdard, New Delhi-110062, India.

<sup>b</sup>Department of Medical Elementology and Toxicology, School of Chemical and Life Sciences (SCLS), Jamia Hamdard, New Delhi-110062, India.

<sup>c</sup>Centre for Transgenic Plant Development (CTPD), Department of Biotechnology, School of Chemical and Life Sciences (SCLS), Jamia Hamdard, New Delhi-110062, India.

<sup>d</sup>School of Pharmacy and Biomedical Sciences, University of Central Lancashire, Preston, United Kingdom.

<sup>e</sup>Department of Chemistry, School of Chemical and Life Sciences (SCLS), Jamia Hamdard, New Delhi-110062, India.

<sup>f</sup>Department of Biochemical Engineering and Biotechnology, Indian Institute of Technology Delhi, New Delhi-110016, India.

#### \*Author to whom correspondence should be addressed:

Professor (Dr.) Farhan Jalees Ahmad

Address: Department of Pharmaceutics, School of Pharmaceutical Education and Research, Jamia Hamdard, New Delhi-110062, India.

Email id: fjahmad@jamiahamdard.ac.in

Phone No: +919810720387

Abstract: Treatment of Ischemic Stroke is inordinately challenging due to its complex aetiology and constraints in shuttling therapeutics across blood-brain barrier. Ropinirole hydrochloride (Rp), a propitious neuroprotectant with anti-oxidant, anti-inflammatory, and anti-apoptotic properties (3A) is repurposed for remedying ischemic stroke and reperfusion (I/R) injury. The drug's low bioavailability in brain however, limits its therapeutic efficacy. The current research work has reported sub-100 nm gamma-L-Glutamyl-L-Cysteine coated Human Serum Albumin nanoparticles encapsulating Rp (C-Rp-NPs) for active targeting in ischemic brain to encourage in situ activity and reduce unwanted toxicities. Confocal microscopy and brain distribution studies confirmed the enhanced targeting potentiality of optimized C-Rp-NPs. The pharmacokinetics elucidated that C-Rp-NPs could extend Rp retention in systemic circulation and escalate bioavailability compared with free Rp solution (Rp-S). Additionally, therapeutic assessment in transient middle cerebral occlusion (tMCAO) model suggested that C-Rp-NPs attenuated the progression of I/R injury with boosted therapeutic index at 1000 times less concentration compared to Rp-S via reinstating neurological and behavioral deficits, while reducing ischemic neuronal damage. Moreover, C-Rp-NPs blocked mitochondrial permeability transition pore (mtPTP), disrupted apoptotic mechanisms, curbed oxidative stress and neuroinflammation, and elevated dopamine levels post tMCAO. Thus, our work throws light on fabrication of rationally designed C-Rp-NPs with enormous clinical potential.

**Keywords:** Brain targeted drug delivery, Human serum albumin nanoparticles, Ischemic stroke and reperfusion injury, Mitochondria, Neuroprotection, Ropinirole hydrochloride.

#### 1. Introduction

Stroke is the foremost cause of morbidity and ranked second for mortality, globally [1]. Among different kinds, ischemic stroke (IS) is the commonest (87%), often distinguished as an occlusion in cerebral blood flow owing to thrombus or embolus, thereby, instigating lack of perfusion of tissues and oxygen supply, subsequently, hindering cellular metabolism. Currently, the only clinical approach recommended by Food and Drug Administration (FDA) for IS therapy is focused on thrombolysis *via* early revascularisation by recombinant tissue plasminogen activator (rtPA), so as to protect neuronal tissue in the penumbra as much as feasible. It is administered within 3-4 hours from the onset of stroke. This gold standard treatment, however, merely aids 3-5% of stroke patients because of its narrow treatment window and exacerbates hemorrhagic risks [2]. Moreover, restoration of vascular supply in ischemic tissue further amplifies the ischemic damage, leading to ischemia/reperfusion (I/R) injury, that further sets off a chain reaction of events, *viz.* blood-brain barrier (BBB) leakage, cerebral edema, calcium burden, glutamate excitotoxicity, oxidative stress, inflammation, mitochondrial perturbation, and apoptosis [3]. Hence, neuroprotectants that can target multifarious pathophysiological events hold attractive potential in averting I/R injury.

The ever-increasing evidence from fundamental and clinical experiments has unraveled the decisive role of mitochondria in the pathophysiology of numerous neurodegenerative diseases, including stroke. Due to their ineluctable role in energy homeostasis, reactive oxygen species (ROS) formation, and apoptotic pathways, mitochondria are vulnerable to various insults. The foremost event in ischemic stroke is the interruption of the electron transport chain (ETC) resulting in disruption of mitochondrial membrane potential (MMP) and synthesis of adenosine triphosphate (ATP). Upon reperfusion, the ischemic injury is intensified as a repercussion of augmented oxidative burden with surplus ROS in mitochondria, culminating in diminished ETC activity and approving the opened state of mitochondrial permeability transition pore (mtPTP). Moreover, ROS generation promotes lipid peroxidation, protein, and deoxyribonucleic acid damage, eventually triggering neuronal cell dysfunction and death. Another event accompanied by ischemic insult is neurotransmitter-induced excitotoxicity leading to excess accumulation of Ca<sup>2+</sup> in the cytosol and causing mitochondrial swelling as well as permeabilization. It liberates numerous apoptotic factors i.e., cytochrome c (cyt-c) and apoptosis-inducing factors (AIF) thereby, assuring apoptotic neuronal death [4]. So, sustaining mitochondrial integrity in I/R injury is of critical importance for assuring neuronal functioning and recovery. For this reason, therapeutic interventions conferring neuroprotection via mitochondria could be a promising tool for the management of I/R injury [5].

Henceforth, Ropinirole (Rp), a dopamine receptor (D3/D2) agonist is repurposed as a potential drug for the possible mitochondrial-mediated neuroprotection and treatment of I/R injury. It is already approved by US FDA for the treatment of Restless Leg Syndrome and Parkinson's disease [6]. The neuroprotective effects of Rp are predominantly elicited through the 3A approach, *viz*. "anti-oxidant, anti-inflammatory and anti-apoptotic" thus targeting multitudinous pathways [7,8]. Despite myriad benefits, Rp has certain shortcomings such as oral therapy-associated adverse effects and low oral bioavailability due to hepatic first-pass effect (CYP1A2) [9]. It is also worthwhile to mention that to date, various neuroprotectants that have shown affirmative outcomes in preclinical research, have failed in clinical trials. This failure is ascribed to the paucity of their safety and efficacy. Additionally, the critical limitation complying with the ineffectiveness of the conventional treatment modalities is the presence of

insuperable BBB that offers resistance to the shuttling of potent neuroprotectants in the ischemic brain. Thus, the aforesaid resistances highlight the inevitability of fabricating drug delivery strategies that can be selectively targeted to ischemic neuronal cells, consequently, affording a higher clinical potential [2].

Acting upon the aforesaid rationale, we fabricated ligand-linked Human Serum Albumin (HSA) based nanoformulation of Rp in I/R injury utilizing the 3A approach. HSA was picked as a protein carrier owing to its easy accessibility, non-toxic nature, water-solubility, nonimmunogenicity, biodegradability, and great amenability for surface decoration with apposite ligand to enhance targeting as well as stability of nanoparticles [10]. It is already permitted by US FDA and used in nanoformulation of paclitaxel, for cancer therapy [11]. Further, protein could be degraded into peptides via innate enzymes, unlike chemical-synthesized nanoparticles that could gather in the body and be degraded into toxic products [10]. It is realized that receptor-mediated drug delivery is the most effective strategy to penetrate the intact BBB and enable the neuroprotectants to enter the brain [12]. Nowadays, several shuttling peptides have been grabbing attention for brain-targeted drug delivery in regard to their non-immunogenicity, cost-effectiveness, and enhanced chemical stability. We ascertained glutathione as one of them reaching a progressive stage en route to clinical application [13]. Thus, for the surface vectorization of Rp-NPs, gamma-L-Glutamyl-L-Cysteine (γ-L-Glu-L-Cys), a dipeptide, and glutathione-precursor, was selected as a probable binding partner of N-methyl-D-aspartate receptor (NMDAR) using molecular docking technique for brain targeted delivery of Rp in I/R injury. Their transferring across the BBB could be assisted through receptor-mediated endocytosis [12]. This might augment the clinical efficacy of C-Rp-NPs by delivering Rp to the ischemic neurons, thereby, overcoming off-target toxicities. At the same time, it might reduce the dose of the Rp and thus, contribute towards cost-effective nanoformulation by strictly adhering to patient compliance.

In this study, we integrated the Rp entrapped in HSA nanoparticles coated with γ-L-Glu-L-Cys, a shuttling peptide, aiming towards the development of a smart brain targeted drug delivery system (designated as C-Rp-NPs) in I/R injury (Fig. 1). Upon intraperitoneal injection of rhodamine B loaded γ-L-Glu-L-Cys coated HSA-NPs (C-Rd-B NPs), mimicking C-Rp-NPs in Wistar rats, the confocal microscopy revealed enhanced active targeting ability of the nanoparticles in the brain in contrast to Rd-B NPs and free Rd-B solution (Rd-B S). *In vivo* pharmacokinetic studies disclosed improved bioavailability and longer retention of Rp from C-Rp-NPs in systemic circulation with respect to Rp-S. *In vivo* therapeutic assessments demonstrated that C-Rp-NPs aided in restoring neurological as well as behavioral deficits by attenuating mitochondrial dysfunction through blocking of mtPTP, derailing apoptotic mechanisms, and alleviating oxidative stress as well as neuroinflammation with a boosted therapeutic index at 1000 times less concentration compared to free Rp-S. Because of the clinical pertinence of this work, we envisage that the verified C-Rp-NPs impart a pioneering outlook for the treatment of I/R injury and thus, have an attractive prospect for translation.

#### 2. Materials & methods

#### 2.1. Chemicals and reagents

Ropinirole hydrochloride (Rp) was provided ex-gratia by Wockhardt Ltd. (Mumbai, India). Bovine serum albumin (BSA), Butylated hydroxytoluene (BHT), 3,3'-Diaminobenzidine (DAB), Dibutylphthalate Polystyrene Xylene (DPX), 2,7-Dichlorodihydrofluorescein diacetate (DCFDA), N-(-3-Dimethylaminopropyl)-N'-ethylcarbodiimide hydrochloride

(EDC), Ethylenediaminetetraacetic acid (EDTA), Ethylene glycol-O,O'-bis(2-aminoethyl)-N,N,N',N'-tetraacetic acid (EGTA), gamma-L-Glutamyl-L-Cysteine (γ-L-Glu-L-Cys), 4-(2-hydroxyethyl)-1-piperazineethanesulfonic acid (HEPES), Human serum albumin (HSA), ortho-Phosphoric acid (OPA), Rhodamine B dye, Sodium dodecyl sulfate (SDS), Thiobarbituric acid (TBA), Tetramethylrhodamine ethyl ester (TMRE), and 2,3,5-Triphenyltetrazolium chloride (TTC) were purchased from Sigma-Aldrich (St. Louis, MO, USA). Absolute Ethanol (99.9%) was supplied by Changshu Hongsheng Fine Chemical Co. Ltd. (China). The two-site sandwich ELISA kits of TNF-α, IL-1β and Dopamine (DA) were acquired from Abbkine Inc., China. Clarity-ECL plus western blotting reagent was purchased from Bio-Rad, Hercules, CA, USA and Polyvinylidene difluoride (PVDF) membrane was purchased from Merck-Millipore, Mumbai, India. Other chemicals and solvents with highgrade purity were obtained from Merck Ltd. (Mumbai, India).

#### 2.2. Animals

Male Wistar rats ( $325\pm25$  g, 12-14 weeks old) were supplied by the Central Animal House Facility, Jamia Hamdard, New Delhi, India. Experimental animals were placed in an isolated environment (temperature  $23\pm2^{\circ}$ C, relative humidity  $65\pm10\%$ , and 12 h light/dark cycle). Animals were permitted free access to a standard rodent diet and RO water ad-libitum. The surgical, as well as experimental protocols, were conducted adhering to the guidelines approved by the Institutional Animal Ethics Committee (IAEC) of Jamia Hamdard (Project No. 1588; Registration No. 173/GO/ReBi/S/2000/CPCSEA).

## 2.3. Synthesis and optimization of γ-L-Glu-L-Cys coated HSA-NPs encapsulating Rp

HSA-based nanoparticles entrapping Rp (Rp-NPs) were prepared employing the desolvation technique, formerly reported by Jahanban-Esfahlan et al. (2016), with minor modifications [14]. Primarily, HSA (protein-based polymer) and Rp were taken in a mass ratio of 8:1 (160 mg and 20 mg, respectively). Thereafter, HSA was dissolved in 3 mL, whereas Rp was dissolved in 1 mL Milli-Q water, respectively. The aqueous solution of Rp was then added drop by drop to the aqueous solution of polymer and the mixture was incubated for 1 hour under continuous stirring (600 rpm). This was followed by the drop-wise addition of 62.5% v/v ethanol to the aforesaid mixture at a rate of 1 mL/min under constant stirring (1250 rpm). The appearance of slight opalescence at the end-point of ethanol indicated the formation of nanoparticles. Subsequently, an aqueous solution of EDC (1% w/v in 0.5 mL Milli-Q water) was added to the obtained unstable nanodispersion for the stabilization of nanoparticles. Hence, the concentration of HSA and Rp taken for synthesis was 22.86 mg/mL and 2.86 mg/mL, respectively in the 7 mL of the nanodispersion. Next, the Rp-NPs were collected via centrifugation using Amicon® Ultra-15 Centrifugal Filter Devices with cut-off 10 kDa (Millipore, Ireland) and purified with Milli-Q water by exposing to 2 cycles of centrifugation (Eppendorf AG, Hamburg, Germany) at 4,000 rpm for 30 and 15 min, respectively. The filtrate and retentate were separately collected after centrifugation. The filtrate was quantified for free Rp concentration using reverse-phase high-performance liquid chromatography (RP-HPLC, Waters Co., Milford, MA, USA). The mobile phase comprised of Solvent A/Solvent B (65:35 v/v) [Solvent A (methanol/0.05 M ammonium acetate buffer, pH 7, 80:20 v/v)] and Solvent B [HPLC grade water] with a flow rate of 0.6 mL/min [15]. The detection wavelength was 250 nm. The DL (%) was determined by making use of a standard calibration curve of Rp. The DL (%) was calculated using the following formula:

$$DL (\%) = \frac{Wi - Wf}{Wt} \times 100$$

where, Wi, Wf, and Wt signify initial amounts of Rp, amount of Rp in filtrate, and the total weight of the materials utilized for the fabrication of Rp-NPs. The experiment was performed in triplicate and results were presented as mean value  $\pm$  SD.

The above-mentioned procedure of Rp-NPs was statistically optimized using Box-Behnken Experimental Design (Design-Expert 11.1.0, State-Ease Inc., Minneapolis, USA) (for details of the procedure, please refer to the Supporting information, *section 1.1*).

Finally, the optimized Rp-NPs were subjected to the surface-decoration by a glutathione-precursor,  $\gamma$ -L-Glu-L-Cys. In this process, the volume of the retentate attained was dispersed in 7 mL of Milli-Q water. Thereafter,  $\gamma$ -L-Glu-L-Cys (3% w/w of polymer) was added to the optimized Rp-NPs and incubated for 1 h under continuous stirring (800 rpm) [16]. Later, the uncoated  $\gamma$ -L-Glu-L-Cys was eliminated from the above mixture *via* centrifugation and  $\gamma$ -L-Glu-L-Cys coated Rp-NPs (C-Rp-NPs) procured, were redispersed in 7 mL of Milli-Q water. All of the above procedures were operated under room temperature.

Lastly, 4% w/v sorbitol was added to the dispersed C-Rp-NPs and this mixture was further, lyophilized in a freeze dryer (Lab Conco., USA) to achieve free-flowing powder. The final formulation was kept in tight containers at 4°C until further use.

For the preparation of fluorescent-labeled nanoparticles, Rhodamine B dye was used as a fluorescent probe. 0.03% w/v of rhodamine-B dye (Rd-B) was dissolved in Milli-Q water and loaded in HSA-NPs and  $\gamma$ -L-Glu-L-Cys coated HSA-NPs utilizing the aforementioned process of preparing Rp-NPs and C-Rp-NPs to generate Rd-B NPs and C-Rd-B NPs, respectively [17].

#### 2.4. Physicochemical characterization

The average hydrodynamic diameter, polydispersity index (PDI), and ζ potential of Rp-NPs, C-Rp-NPs, Rd-B NPs, and C-Rd-B NPs were detected by Zetasizer (Nano ZS, Malvern Instruments, Malvern, UK). The morphological characteristics of C-Rp-NPs were determined using TEM (JEM-1400 Flash, JEOL, Japan) and SEM (FESEM, Jeol JSM-7800F Prime, Japan). Further, the coating of γ-L-Glu-L-Cys on optimized Rp-NPs was evaluated *via* Fourier transformed infrared (FT-IR) spectroscopy. The spectra of γ-L-Glu-L-Cys and C-Rp-NPs were recorded over the range of 4000–1200 cm<sup>-1</sup> using an FT-IR/NIR spectrometer (PerkinElmer, USA). Lastly, the *in vitro* release profiles of Rp from Rp-S (free drug solution), Rp-NPs, and C-Rp-NPs were investigated under sink conditions employing the dialysis bag method in phosphate buffer saline (PBS) at pH-4.0 and 7.4 in order to simulate the physiological conditions of ischemic brain and plasma, respectively [18]. Moreover, the Rp release profile was applied to different kinetic models, *viz*. zero order, first order, Higuchi, Hixon-Crowell, and Korsmeyer-Peppas models, and the R<sup>2</sup> (regression co-efficient) value was calculated for deciding the best-fit. For detailed methodology, please refer to the Supporting information, *section 1.2*.

## 2.5. In vitro cytotoxicity assay

#### 2.5.1. Neuro-2a cell culture

The mouse brain-derived neuroblastoma cells, Neuro-2a were grown in Dulbecco's Modified Eagle Medium (DMEM) supplemented with 10% v/v fetal bovine serum, 1% v/v antibiotic solution (Penstrap), and 200 mM L-glutamine. Cells were incubated at 37°C with 5% CO<sub>2</sub> [19].

## 2.5.2. Cytotoxicity assay

A mitochondrial enzyme-dependent reaction of 3-(4,5-Dimethyl-2-thiazolyl)-2,5-diphenyl-2H-tetrazolium bromide (MTT) was performed to assess the cytotoxicity of the prepared nanoparticles. Neuro-2a cells were seeded into a 96-well plate at a density of  $15\times10^3$  cells/well. Freshly prepared nanoparticle suspensions (Rp solution, Rp-S; HSA-NPs without Rp, HSA-NPs; Rp-NPs; and C-Rp-NPs) were added to the cultures at escalating doses (5, 10, 15, 20, and 25  $\mu$ g/mL) and evaluated for toxicity after 24 h of incubation. The medium was discarded at the termination of the exposure time, and the cells were rinsed once with PBS (pH 7.4) before being re-suspended in fresh culture medium and the MTT reagent (200  $\mu$ L/well). Following 3 h, the culture medium was withdrawn and dimethyl sulfoxide (200  $\mu$ L) was added to aid in the dissolution of the produced formazan crystals. The plates were appropriately processed at this time to detect absorbance at 540 nm. The experiment was conducted in triplicate and the results were presented as mean value  $\pm$  SD. As a positive control, cells that had not been treated were used. Finally, the cell viability (%) was computed using the following formula [20]:

Cell Viability (%) = 
$$\frac{\textit{Absorbance of cells treated with nanoparticles}}{\textit{Absorbance of positive control}} \times 100$$

## 2.6. Uptake study of Rd B-labeled NPs in brain

The authentication of the targeting potential of  $\gamma$ -L-Glu-L-Cys coated HSA-NPs as carriers for neuroprotectants to the brain was assessed *via* confocal laser scanning microscopy (CLSM). The brains were longitudinally sectioned for the preparation of slides at 6 h after the intraperitoneal (*i.p.*) administration of Rd-B solution (Rd-B S), Rd-B NPs, and C-Rd-B NPs formulations in male Wistar rats. The slides were then, observed under CLSM equipped with a confocal head, TCS SPE, and a 63 water immersion objective (Leica, Germany) at  $\lambda$ ex 488 nm and  $\lambda$ em 560 nm (red fluorescence). Thereafter, the images were processed by LASAF software (Leica, Germany) and compared. The relative fluorescence intensity (F%) produced by various nanoparticles in brain sections was computed by the formula [21]:

Relative fluorescence intensity (F%)=  $\Delta F/F_0 \times 100$ 

where,  $F_0$  is basic fluorescence intensity,  $\Delta F$  is change in fluorescence intensity produced by nanoparticles in brain sections subtracted by basic fluorescence intensity.

#### 2.7. Pharmacokinetics and brain distribution study

Sixty-three male Wistar rats were randomly divided into three groups (Rp-S, Rp-NPs, and C-Rp-NPs) and three animals were allocated to each time point per group, *i.e.*, 0.5, 1, 2, 4, 8, 12, and 24 h for the study. The Rp solution (Rp-S) was administered *i.p.* at a dose of 10 mg of Rp/kg b.wt. (3.25 mg/mL), whereas Rp-NPs and C-Rp-NPs dispersed in Milli-Q water were administered *i.p.* at a dose equivalent to 10 mg of Rp/kg b.wt. Hence, the concentrations of Rp-NPs and C-Rp-NPs taken in the injected solutions were 97.3 mg/mL and 101.25 mg/mL, respectively. The concentration of Rp in plasma was determined *via* withdrawing the blood

samples (0.5 mL) from retro-orbital choroid plexus into the heparinized tubes at each of the pre-decided time points after the administration. The blood samples were subjected to centrifugation at 5000 rpm for 15 min to extract plasma.

In a brain distribution study, the animals were sacrificed at pre-selected time points, *viz.* 3, 6, and 9 h to collect brains after acquiring the plasma. For this, the rats were euthanized followed by the cutting of their skulls by means of surgical scissors to isolate their brains. After the removal of brains, their integrity was ensured and they were quickly washed with ice-cold PBS to get rid of surface blood. Each of the brain tissue was weighed and succeeded by its homogenization with a tenfold volume of Milli-Q water. All plasma and brain homogenate samples were stored at -80°C until analysis.

The contents of Rp in plasma and brain homogenate samples taken from rats administered with Rp solution, optimized Rp-NPs, and C-Rp-NPs were quantified using UPLC-MS/MS system (Waters Co., MA, USA) by liquid-liquid extraction method (for method details, please refer to Supporting information, *section 1.3*). C<sub>max</sub>, T<sub>max</sub>, AUC<sub>0-t</sub>, T<sub>1/2</sub>, and clearance were measured exploiting the Microsoft Excel Addins-PK Solver and Pk1.Pk2 [22].

## 2.8. Transient Middle Cerebral Artery Occlusion Model (tMCAO Model)

The ameliorated transient middle cerebral artery occlusion (tMCAO) was employed for inducing focal cerebral ischemia and reperfusion as established earlier [6]. The method is elaborated in detail in the Supporting Information, *section 1.4*.

## 2.8.1. Experimental design

Ninety experimental rats were randomly allotted to six groups (n=15): Group (I): Sham group, *i.p.* administered with 0.9% sterile normal saline; Group (II): tMCAO group, *i.p.* administered with blank γ-L-Glu-L-Cys coated HSA-NPs; Group (III): tMCAO + Rp-S (20 mg/kg b.wt.) served as standard treatment; Group (IV): tMCAO + C-Rp-NPs 0.001 (1 μg/kg b.wt.); Group (V): tMCAO + C-Rp-NPs 0.01 (10 μg/kg b.wt.) and Group (VI): tMCAO + C-Rp-NPs 0.02 (20 μg/kg b.wt.). Blank γ-L-Glu-L-Cys coated HSA-NPs, Rp-S and C-Rp-NPs were dissolved in 0.9% sterile normal saline and administered *i.p.* at 6, 12, and 18 h post-occlusion. Dose regime along with the route of administration was chosen in agreement with the previous literature [6]. Neurobehavioral tests were performed at 24 h following tMCAO. Subsequently, the animals were deeply anesthetized by an overdose of ketamine and xylazine for their sacrifice *via* cervical dislocation needed for the estimation of infarct volumes. Additionally, the frontal cortex of their brains was isolated for biochemical and molecular analysis.

# 2.9. Assessing cerebral ischemia/reperfusion injury via neurological deficits, behavioral parameters, and infarct volume

The neurological deficit score was evaluated in a blind manner at 24 h post-tMCAO. The assessment of neuroscore involved a four-point scale established by Bederson *et al.* (1986) [23] consisting of 0 grade: no deficits; 1 grade: flexion of forelimb; 2 grade: reduced resistance to lateral push and flexion of forelimb without circling; and 3 grade: reduced resistance to lateral push and flexion of the forelimb with circling. The behavioral parameters were investigated for analyzing motor impairment and muscular strength of experimental rats post-tMCAO injury *via* narrow beam walk and grip strength test. The details of these investigations are provided in the Supporting information, *section 1.5*. After the aforesaid neurological analyses,

experimental rats were sacrificed and their brains were isolated to obtain coronal slices (2 mm thick) through the rat brain matrix. The sections were then, stained with 2% of 2,3,5-triphenyltetrazolium chloride solution (TTC) followed by overnight fixation with 10% formalin solution. Lastly, the infarct volume was computed *via* Image-J (Wayne Rasband, NIH, USA) [24].

### 2.10. Biochemical analyses

## 2.10.1. Preparation of tissue and isolation of mitochondria

Following the euthanization of experimental animals, injured penumbra tissue was cautiously dissected from the ipsilateral hemisphere employing a rat brain slicer matrix (BSRAA002, Zivic Instruments, Pittsburgh, PA, USA) for biochemical analysis. The penumbra tissue was then, homogenized in ice-cold 0.1 M phosphate buffer (pH 7.4) to acquire 10% w/v homogenate and further centrifuged at 21, 380×g at 4°C for 20 min to obtain post-mitochondrial supernatant (PMS). Lastly, the homogenate and PMS were stored at -80°C for further analysis. Mitochondria were extracted *via* dissecting the frontal cortex of the brain and exploiting differential centrifugation methodology, previously described by Andrabi *et al.* (2017) (refer Supporting information, *section 1.6*) [4]. All mitochondrial oxidative stress biomarkers were evaluated on a similar day prior to the mitochondrial isolation.

#### 2.11. Determination of oxidative stress biomarkers

Oxidative stress biomarkers generally include glutathione (GSH), lipid peroxidation (LPO), mitochondrial ROS (Reactive Oxygen Species) level and mitochondrial membrane potential ( $\Delta\psi m$ ). The GSH and LPO were determined from PMS and homogenate, respectively, whereas mitochondrial ROS and  $\Delta\psi m$  were determined from isolated mitochondria. GSH assay was performed as stated by Andrabi *et al.* (2017) [4]. The result was given as  $\mu moles$  of GSH/g tissue using molar extinction coefficient (MEC) as  $1.36 \times 10^4$  M $^{-1}$  cm $^{-1}$ . For LPO assay, a method explained by Chaudhary and Parvez (2012) was employed with some modifications [25]. Concisely, the homogenate samples were subjected to incubation with 10 mmol/L BHT, 0.67% TBA, and 1.0% OPA for 45 min at 90°C. Post-incubation, the reaction mixture was centrifuged at 3,000 rpm for 15 min followed by its photometric measurement at 535 nm. The results were presented as nmoles of TBARS formed/h/g tissue using a MEC of  $1.56 \times 10^5$  M $^{-1}$  cm $^{-1}$ . Mitochondrial ROS and  $\Delta\psi m$  were evaluated by flow cytometry by making use of DCFDA and TMRE dyes, respectively. The flow cytometric acquirement of fluorescent intensities from 10,000 events was completed using BD-LSR II. The histograms were created and statistical analysis was accomplished with the aid of FACS-DIVA software.

#### 2.12. Analysis of ATP

The ATP content was quantified using an ATP assay kit (Elabscience, #E-BCK157-S) in accordance with the guidelines provided by the manufacturer. In this protocol, the brain tissue was first homogenized in double-distilled water followed by its incubation in a water bath for 30 min at  $90^{\circ}\text{C}$ . Succeeding incubation, the brain homogenate was centrifuged for 10 min at  $10,000\times g$  and the supernatant collected, was added in the substrates, mixed, and transferred to 96-well plates for colorimetric analysis.

## 2.13. Estimation of dopamine and inflammatory cytokine levels

Dopamine as well as inflammatory cytokine levels, viz. TNF- $\alpha$  and IL-1 $\beta$  were calculated at 24 h following cerebral ischemia/reperfusion injury. The levels of dopamine and aforementioned cytokines were measured in brain homogenates using ELISA kits. The assay was conducted abiding by the instructions given by the manufacturer.

## 2.14. Immunohistochemistry for D2 receptor (D2R)

The immunohistochemical staining was carried out following the formerly documented protocol [26]. Post-reperfusion, the experimental animals were anesthetized and transcardially perfused with chilled saline succeeded by fixation of brain tissues with 4% paraformaldehyde and embedding in paraffin wax. Coronal slices (5 µm) were cut from paraffin-embedded tissues with a microtome. Slices were de-paraffinized in xylene and dehydrated in graded ethanol before being boiled in 10 mM sodium citrate buffer (pH 6.0) for antigen retrieval. After washing, slices were blocked and incubated overnight at 4°C with a primary antibody against D2R (1:200; Genetex; USA). Following washing, secondary antibody (1:1000; Cell Signalling, Beverly, USA) incubation and staining with DAB as well as hematoxylin were done. Finally, the samples were mounted with DPX and examined under a microscope at a magnification of 20x (Zeiss, Oberkochen, Germany). The semi-quantitative approach was adopted to analyze immunohistochemistry staining. Based on the diffuseness of DAB, sections were evaluated as: 0 = negligible staining, 1 = 25% staining, 2 = 25-50% staining, 3 = 50-75% staining, and 4 = 60-75% staining>75% staining. Likewise, based on the staining intensity, sections were graded as: 0 =negligible staining, 1 = faint but detectable staining, 2 = distinct staining, and 3 = intensestaining. The final scores were acquired by adding the diffuseness and intensity ratings of the blinded examiner.

## 2.15. Western blotting

After the collection of the frontal cortex of brain tissue, it was exposed to homogenization in ice-cold lysis buffer constituted of a protease and phosphatase inhibitor cocktail (Sigma-Aldrich, USA) using a hand homogenizer as described by Sanderson et al. (2013) with few modifications [27]. Briefly, lysed brain samples were centrifuged at 20,000×g for 30 min at 4°C. Later to centrifugation, Bradford assay was used for quantifying the protein, which was separated by 10-15% sodium dodecyl sulphate-polyacrylamide gel (SDS-PAGE) and successively transferred to PVDF membranes. Thereafter, the membranes were blocked with 5% non-fat dry milk and incubated with primary antibodies, viz. Bcl-2 (1:1000; sc-7382, Santa Cruz Biotechnology), cyt-c (1:1000; 136F3, Cell Signaling Technology), β-actin (1:3000; A01010, Abbkine), Bax (1:1000; sc-439, Santa Cruz Biotechnology) and COX-IV (1:1000, #GTX114330, GeneTex) at 4°C overnight. The next day, membranes were washed three times with PBST (phosphate buffer saline, pH-7.5, along with 0.05% Tween 20) followed by its incubation with horseradish peroxidase-conjugated secondary antibodies (1:10,000; antirabbit, Invitrogen; anti-mouse, Abbkine) at room temperature for 2 h. The bands were detected by enhanced chemiluminescence and densitometric analysis was performed by Image-J software 1.46r (Wayne Rasband, NIH, USA).

#### 2.16. Examination of histopathological alterations

For histological analyses, hematoxylin and eosin (H and E) staining was performed as previously described. The animals were anesthetized and transcardially perfused with 0.9% saline and then with 4% paraformaldehyde at 24 h after I/R injury. Thereafter, the brain was quickly removed and fixed with 10% formalin. Later, the paraffin-embedded brain samples were sliced into  $5~\mu m$  thick coronal sections and subsequently, stained with H and E. A

microscope (Zeiss, Oberkochen, Germany) was used to visualize these sections, which were then quantified by Image J 1.46r software (Wayne Rasband, NIH, USA) [28].

#### 2.17. Statistical analysis

All the data of pharmacodynamic studies (behavioral, biochemical, and immunoblots analyses) were stated as mean  $\pm$  standard error of mean (SEM). The results of the aforesaid studies were obtained from three independent experiments. Comparisons amid multiple groups were evaluated with one-way analysis of variance (ANOVA) followed by Tukey's post hoc test, whereas the statistical analysis of data was accomplished by Graph Prism 5 Software (GraphPad Software Inc., San Diego, CA, USA). Significant differences were defined as *P*-value < 0.05.

#### 3. Results and discussion

3.1. Synthesis, optimization, and characterization of  $\gamma$ -L-Glu-L-Cys coated HSA-NPs encapsulating Rp

HSA has a remarkable potential to bind several drugs owing to the presence of different drug binding sites [29], hence, it was employed in our study for the fabrication of Rp-NPs. For its preparation, the desolvation technique was used due to its simplicity, robustness, and reproducibility [30]. The stabilization of HSA-NPs is an essential step usually achieved *via* a chemical cross-linking strategy involving glutaraldehyde. However, the use of glutaraldehyde is controversial because of its intrinsic toxicity and persistence in nanoparticulate structures. Hence, a zero-space cross-linking agent, EDC was utilized to form peptide bands amongst amine and carboxyl groups for the stabilization of Rp-NPs. This reaction generates urea as a by-product which can be easily detached from nanoparticulate structures through centrifugation. Additionally, EDC reduces the reaction time in comparison to glutaraldehyde from overnight to 3 h [14].

The next step was the optimization of the Rp-NPs systematically employing Quality by Design (QbD) principles, which enabled improved knowledge of the product and process parameters on the formulation performance. Thus, a 3-factors, 3-levels containing Box-Behnken Design (BBD) was used to prepare the Rp-NPs where, drug: polymer ratio, ethanol volume (mL), and amount of cross-linker (mg) were taken as the critical material attributes (CMAs), whereas particle size, PDI, and drug loading (%) as critical quality attributes (CQAs). Design-Expert software (Design-Expert 11.1.0, State-Ease Inc., Minneapolis, USA) was employed to create thirteen runs for the preparation and optimization of Rp-NPs. The values of response variables for the above experiments are summarised in the Supporting information, Table S1.

Here, the investigational data attained, as per BBD, showed good fitting to the nonlinear second-order model equation which is presented as follows:

$$Y = \beta_0 + \beta_1 X_1 + \beta_2 X_2 + \beta_3 X_1 X_2 + \beta_4 X_1^2 + \beta_5 X_1 X_2^2 + \dots + \beta_n X_m X_n$$
 (1)

The above data analysis implied the feasibility of the model with the current information, as approved *via* ANOVA model *P*-value <0.05, R<sup>2</sup> close to 1, insignificant lack of fit, and negligible values of predicted error. For each of the response variables, the specifications of several statistical parameters are compiled in (Table S2). Furthermore, a response surface study was implemented utilizing 2D and 3D plots that showed curvature effect, thereby, indicating the interaction amongst the factors.

The 3D-response surface plot in Fig. S1-A (a-c) (in Supporting information) portrays the impact of independent constraints on particle size. Here, negligible influence at all levels of both drug: polymer ratio and cross-linker amount was observed on the values of particle size. Similarly, no effect was perceived on the particle size up to the intermediate levels of ethanol volume. However, a sudden steeper escalation was observed with increasing the volume of ethanol from intermediate to highest level. Hence, reduced particle sizes could be acquired at lower levels of ethanol volume.

The 3D-response surface plot in Fig. S1-B (a-c) depicts the effect of independent constraints on PDI, where a linear inclining trend was noticed in the values of PDI at all the levels of drug: polymer ratio. However, the graph showed a distinct dip in the values of PDI up to the intermediate levels of cross-linker amount followed by a plateau phase. The ethanol volume also exhibited similar observations. Therefore, decreased values of PDI might be attained at the lowest levels of drug: polymer ratio and at intermediate levels of both cross-linker amount and ethanol volume.

The influence of independent constraints on drug loading was portrayed by the 3D-response surface plot in Fig. S1-C (a-b). In this case, a curvilinear and highly pronounced trend was noted with an initial rise in the values of drug loading efficiency from low to intermediate levels of drug: polymer ratio followed by a sharp descending trend. The ethanol volume displayed a curvilinear trend too. However, this trend was marked with a primary declining phase in the values of drug loading until the intermediate levels of ethanol volume consequently, leading to improved loading at the highest levels. The amount of cross-linker indicated minuscule deviations. As a result, improved drug payload could be achieved at intermediate levels of drug: polymer ratio and highest levels of ethanol volume.

The optimized Rp-NPs were chosen via "trading off" numerous CQAs in order to achieve desired objectives. These include minimization of the particle size along with PDI and maximization of drug loading. Here, the weighing and importance were applied to the particle size (a prerequisite for the shuttling of nanoparticles across the blood-brain barrier and its absorption), PDI (measures the degree of heterogeneity of particles in a nanoformulation), and drug loading (a high drug payload is needed for enhanced therapeutic efficacy) based on the critical nature of the response, especially their direct impact on the efficacy of the formulation and the ultimate safety of the patients, hence equal importance (value 3) was assigned to all the three parameters. Table S3 clearly establishes the numerical optimization limits and composition of numerous nanoformulations, accompanied by the values of their analogous desirability functions. Based on the numerical optimization, the formulation with drug: polymer ratio, ethanol volume, and cross-linker amount at coded values of 20.153, 2.509, and 5.046 along with the desirability function of unity were selected as the optimized nanoformulation among several solutions. The optimized Rp-NPs showed an appreciable drug loading of 3.34±0.2% which was quantified using an in-house developed method of HPLC. The average hydrodynamic diameter, PDI, and zeta potential measurements of optimized Rp-NPs based on dynamic light scattering (DLS) were found to be 72.04±0.73 nm, 0.431±0.05, and -20.3±0.32 mV, respectively (Fig. S2A, B). The validation of the QbD methodology was evaluated by making use of the prepared check-point formulations. These formulations unveiled close similarity between the observed and predicted responses of CQAs with the overall percent prediction error was less than 5%.

It is a well-known fact that glutathione, an antioxidant is often transported in the brain via glutamate receptors (N-methyl-D-aspartate, NMDA and α-amino-3-hydroxy-5-methyl-4isoxazolepropionic acid, AMPA) that are copiously expressed at the BBB [12]. Therefore, it has been enormously exploited as a shuttle peptide of BBB for the transfer of numerous therapeutic cargos in the brain [13]. We found that y-L-Glu-L-Cys is a non-toxic type of cysteine and a precursor to an endogenous tripeptide, i.e., glutathione. Hence, in our prior findings, we have identified the competency of γ-L-Glu-L-Cys (having more than 95% structural resemblance to glutathione) as a ligand of NMDAR accordant with its high binding affinity (-6.3 kcal/mol) than glutathione (-5.8 kcal/mol) and selectivity to the ligand-binding pocket of NMDAR [12]. Thus, we expected γ-L-Glu-L-Cys-succoured boosted therapeutic index in the ischemic brain and consequently, reduced systemic toxicity by virtue of receptormediated endocytosis in I/R injury. Building upon this hypothesis and encouraged by the outcomes of molecular docking studies as discussed above, we had coated γ-L-Glu-L-Cvs on the surface of optimized Rp-NPs to develop C-Rp-NPs. This surface-coating could be ascribed to the non-covalent interactions (e.g., hydrophobic effect, hydrogen bonding) and electrostatic interactions on account of functional group viz. carboxyl and amine groups on HSA [31]. Postcoating, the DLS analysis revealed average hydrodynamic diameter of the optimized C-Rp-NPs was  $73.37\pm1.43$  nm (Fig. 2A) and the  $\zeta$  potential was augmented to  $-25.7\pm0.57$  mV (Fig. 2B) pointing towards electrostatic and steric stabilization of colloidal dispersions with respect to the Rp-NPs. The relatively increased surface  $\zeta$  potential suggested that  $\gamma$ -L-Glu-L-Cys was successfully attached to the surface of C-Rp-NPs. To validate the attachment of γ-L-Glu-L-Cys on the surface of optimized Rp-NPs, Fourier transform infrared (FT-IR) spectroscopy measurements were executed. FT-IR spectra of γ-L-Glu-L-Cys depicted characteristic peak of -SH group at 2360 cm<sup>-1</sup>, also identified in C-Rp-NPs further establishing that coating was done efficiently (Fig. S3) [32]. The PDI of C-Rp-NPs was found to be 0.218±0.0045 signifying that the size distribution of developed nanoparticles was fairly narrow [33]. Furthermore, the morphological inspection of the developed and optimized C-Rp-NPs was executed via transmission electron microscopy (TEM) (Fig. 2C) and scanning electron microscopy (SEM) (Fig. 2D). The particles manifested spherical structure with smooth surface and a reduced particle size of ≤100 nm was detected which is favorable for the brain targeting [34] and was analogous with DLS results. Additionally, the average hydrodynamic diameter, PDI, and  $\zeta$ potential of Rd-B NPs were found to be 75.9±0.93 nm, 0.231±0.006, -19.95±0.04 mV (Fig. S4A, C), whereas for C-Rd-B NPs, these were found to be 77.8±1.1 nm, 0.254±0.03, and -26.2±0.72 mV, respectively (Fig. S4B, D). These observations suggest that the Rd-B NPs and C-Rd-B NPs had almost similar physicochemical characteristics as observed in the case of Rp-NPs and C-Rp-NPs, respectively.

Finally, we assessed the time-dependent release behavior of Rp from Rp-S (free drug solution), Rp-NPs, and C-Rp-NPs in PBS at an acidic pH-4.0 and physiological pH-7.4 identifying with the stroke progression, respectively under sink conditions. As apparent from the cumulative drug release *vs* time curve of PBS at pH-7.4, in comparison to Rp-S where 91.36±2.74% of Rp was released within an hour, a burst release of about 59.61±2.04% and 70.1±3.05% was observed for Rp from Rp-NPs and C-Rp-NPs in the initial 1 h followed by a sustained release of approximately 85.01±4.04% and 93.81±3.38% for the next 5 h, respectively (Fig. S5A). This was followed by a plateau phase until 8 h. The similar pattern was observed at PBS (pH-4.0) where Rp from Rp-NPs and C-Rp-NPs exhibited the release of 98.78±2.25% and 97.46±3.41% in 5 h following a burst release of 74.61±2.69% and 67.03±1.94 in the first hour, respectively

while 104.15±3.42% of Rp from Rp-S was released within an hour (Fig. S5B). The relatively rapid release in the first hour of study could be because of the considerable amount of drug that remained on or close to the surface of the Rp-NPs as well as C-Rp-NPs. The next 5 h presents drug release in a sustainably increased fashion, presumably as a result of the longer diffusion path traveled by the drug molecules concentrated within the core of the polymeric matrix [35]. Moreover, the identical release pattern of Rp from Rp-NPs and C-Rp-NPs in PBS at pH-4.0 and 7.4 could possibly be attributed to the hydrophilic nature of the drug (Rp), polymer (HSA), and ligand (γ-L-Glu-L-Cys). Hence, this biphasic release profile of Rp can offer unique benefits in I/R injury as the initial drug release shall provide the coveted therapeutic concentration immediately. Further, sustained delivery of Rp from nanoparticles could minimize the systemic toxicity and enrich the targeting proficiency of nanoparticles, therefore, is preferable in blood circulation [35]. Furthermore, for the clinical management of acute diseases with nanoparticles, in particular stroke, a rapid response/medicament release (59.61±2.04%, 70.1±3.05% in 1 h and 85.01±4.04%, 93.81±3.38% in 6 h) is perhaps desired [36].

The release kinetics of Rp from the Rp-NPs and C-Rp-NPs were analyzed by submitting the release data into different kinetic models (Table S4). The drug release best fits the Korsemeyer-Peppas model and the R² values were deduced to be (0.9221 and 0.9142 for Rp-NPs and C-Rp-NPs at pH-7.4) and (0.8702 and 0.9513 for Rp-NPs and C-Rp-NPs at pH-4.0), respectively. The value of release exponent (n) was found to be (0.108 and 0.094 for Rp-NPs and C-Rp-NPs at pH-7.4) and (0.115 and 0.113 for Rp-NPs and C-Rp-NPs at pH-4.0), respectively suggesting the Fickian diffusional transport of the Rp from Rp-NPs and C-Rp-NPs.

## 3.2. In vitro cytotoxicity assay

Neuro-2a cell lines are becoming a more appealing paradigm for studying cytotoxicity. Because of the existence of neuronal characteristics, it is often employed as an *in vitro* neuron model [37] to assess neurodegenerative disorders such as Ischemic stroke [38], Parkinson's disease [19], Alzheimer's disease [39], neurotoxicity [37], and neurite outgrowth [40]. Hence, the cytotoxicity of Rp-S, HSA-NPs, Rp-NPs, and C-Rp-NPs was evaluated in Neuro-2a cells for 24 h at concentrations ranging from 5-25  $\mu$ g/mL. Cell viability (%) in HSA-NPs, Rp-NPs, and C-Rp-NPs ranged between 100.23 $\pm$ 0.051-87.52 $\pm$ 0.084%, 99.16 $\pm$ 0.026-86.66 $\pm$ 0.017%, and 99.58 $\pm$ 0.015-86.66 $\pm$ 0.021%, respectively at doses ranging from 5 to 25  $\mu$ g/mL. Further, Rp-S showed cell viability (%) of 89.58 $\pm$ 0.011-80.42 $\pm$ 0.006% at concentrations ranging from 5 to 25  $\mu$ g/mL (Table 1). Thus, the foregoing data undoubtedly establish that the Rp-S, HSA-NPs, Rp-NPs, and C-Rp-NPs are non-cytotoxic and biocompatible in nature.

#### 3.3. Uptake study of Rd B-labeled NPs in brain

To investigate whether the synthesized carrier,  $\gamma$ -L-Glu-L-Cys coated HSA-NPs have gained adequate targeting potentiality *in vivo*, the trafficking profile of Rd-B S, Rd-B NPs, and C-Rd-B NPs in the brain was evaluated in male Wistar rats. In view of the overexpression of glutamate receptors at BBB junction, considerably improved uptake efficiency of C-Rd-B NPs in brain slices was confirmed by confocal laser scanning microscopy compared to Rd-B NPs and Rd-B S as presented in Fig. 3A. Quantitatively, the fluorescence intensity of C-Rd-B NPs group was significantly greater *i.e.*, 1.4-folds and 3.34-folds higher than that of Rd-B NPs and Rd-B S in coronal sections following *i.p.* administration, respectively (Fig. 3B). Hence, this data undoubtedly confirm that the substantial penetration capability of C-Rd-B NPs in the brain could be credited to the selective targeting of  $\gamma$ -L-Glu-L-Cys ligand to the NMDA or AMPA

receptors on the BBB. Collectively, our findings implied that the  $\gamma$ -L-Glu-L-Cys coated HSA-NPs as carriers for neuroprotectants could have enormous potential in localizing payloads to the ischemic brain, specifically *via* receptor-mediated endocytosis based uptake mechanism [12,32].

## 3.4. Pharmacokinetics and brain distribution study

The plasma concentration-time curve of Rp after i.p. injection of Rp-S, Rp-NPs, and C-Rp-NPs are illustrated in Fig. 3C. Succeeding a single dose of i.p. administration, Rp-NPs and C-Rp-Nps depicted a protracted circulation time of Rp that can be estimated even after 24 h in plasma. On the other hand, the amount of Rp in plasma of male Wistar rats injected with Rp-S was not detected after 12 h. This could be attributed to the likeness of the i.p. route with the oral route where therapeutic agents may endure hepatic metabolism before getting into the systemic circulation. Besides, a minor i.p. injectate may pass directly into the thoracic lymph [41]. Hence, the entrapment of Rp in HSA-NPs markedly increased the area under the curve (AUC<sub>0-t</sub>) by 2.8-folds, half-life (T<sub>1/2</sub>) by 2.2-folds, and decreased the clearance by 2.4-folds in contrast to Rp-S. However, in comparison to Rp-NPs, C-Rp-NPs showed greater AUC<sub>0-t</sub> and reduced clearance i.e., 4.6- and 3.8-folds, respectively (Table S5). Though, the T<sub>1/2</sub> of C-Rp-NPs was nearly similar to Rp-NPs which could be elucidated via in vitro drug release studies. The observed findings could be attributed to: (i) the long circulation half-life of albumin in the blood that aids in improving the plasma AUC value, thereby endorsing a fairly high concentration of therapeutics in blood for extended intervals [42] and (ii) the sustained-release profile of Rp from Rp-NPs and C-Rp-NPs. Moreover, in the current study, γ-L-Glu-L-Cvs modification appeared to have further influenced the long circulation effect and consequently, AUC<sub>0-t</sub> and clearance. This is in confirmation with previous literature highlighting the role of small targeting peptides in deterring the recognition by RES [43].

Brain distribution was studied in healthy male Wistar rats whose BBB was completely intact to omit the effects of impaired BBB in I/R injury. The variations in brain distribution between Rp-S, Rp-NPs, and C-Rp-NPs at 3, 6, and 9 h after *i.p.* injection are given in Table 2. Compared with the maximum of  $24.45\pm0.92$  ng/mL brain concentration of Rp-S achieved at 3 h, the maximum brain concentrations,  $449.57\pm18.62$  ng/mL and  $2141.97\pm77.29$  ng/mL of Rp-NPs and C-Rp-NPs, respectively were attained at 6 h. At 9 h, the brain concentrations of Rp-S, Rp-NPs, and C-Rp-NPs were fallen to  $4.14\pm0.21$  ng/mL,  $22.89\pm0.63$  ng/mL and  $31.64\pm2.88$  ng/mL, respectively. Thus, as anticipated, C-Rp-NPs exhibited a dramatic increase in Rp accumulation in the brain compared to Rp-NPs and Rp-S, especially at 6 h which is in corroboration with our confocal microscopy results. Hence, the result justifies specific affinity and binding of  $\gamma$ -L-Glu-L-Cys with glutamate receptors on BBB thereby, facilitating  $\gamma$ -L-Glu-L-Cys mediated endocytosis in the brain and is in concurrence with our former published observations [12].

Therefore, with regard to the advancement in pharmacokinetics as well as brain distribution, C-Rp-NPs might escalate therapeutic concentration in the brain and extend circulatory half-life time so as to improve the clinical potential of the drug (Rp). Hence, further studies in the tMCAO rat model were pursued with C-Rp-NPs to investigate its therapeutic efficacy in a dose-dependent manner.

3.5. Effects of C-Rp-NPs on neurological deficits, behavioural parameters and infarct volume in tMCAO rats

Next, we explored the neuroprotective effects of C-Rp-NPs in the tMCAO rat model following the treatment regimen outlined in Fig. 4A. Since, I/R injury is responsible for a series of neurological impairments thereby, upsetting the motor and sensory functionality of the brain owing to the restricted supply of blood in its lateral surface and basal ganglia [44]. Hence, the neuromodulatory effect of C-Rp-NPs was evaluated using neurological deficits, behavioral tests such as narrow beam walk as well as grip strength tests, and infarct size at 24 h following the ischemic reperfusion in reinstating the neurological alterations. These tests were performed in six groups of experimental rats: Group (I): Sham group, *i.p.* administered with 0.9% sterile normal saline; Group (II): tMCAO group, *i.p.* administered with blank  $\gamma$ -L-Glu-L-Cys coated HSA-NPs; Group (III): tMCAO + Rp-S (20 mg/kg b.wt.) served as standard treatment; Group (IV): tMCAO + C-Rp-NPs 0.001 (10  $\mu$ g/kg b.wt.) and Group (VI): tMCAO + C-Rp-NPs 0.02 (20  $\mu$ g/kg b.wt.).

At first, the neurological function was estimated using the neurological deficit score after tMCAO injury in rats. The neuroscore was given with the aid of instructions adopted from Bederson [23]. As shown in Fig. 4B, severe neurological deficits induced by 1/R injury were found in the tMCAO group (P < 0.001) than the sham group. Treatment with Rp-S [20 mg/kg b.wt. (P < 0.001)] and C-Rp-NPs [10 µg/kg b.wt. (P < 0.001)] and 20 µg/kg b.wt. (P < 0.001)] ameliorated neurological deficits significantly, whereas C-Rp-NPs (1 µg/kg b.wt.) showed no significant reduction in the average score.

Then, we evaluated the narrow beam walk test to examine the motor coordination skills of rats and noticed that the tMCAO-subjected rats were incapable of traveling across the narrow beam (P < 0.001) and therefore, took longer than sham rats. On the other hand, post-treatment with Rp-S [20 mg/kg b.wt. (P < 0.001)] and C-Rp-NPs [10  $\mu$ g/kg b.wt. (P < 0.001)] and 20  $\mu$ g/kg b.wt. (P < 0.001)] remarkably enhanced the motor performance and enabled rats to travel across the beam within 60 sec as opposed to tMCAO rats. Conversely, no significant variation was observed at the lowest dose of C-Rp-NPs (1  $\mu$ g/kg b.wt.) in improving motor function abnormalities in rats (Fig. 4C).

Further, we evaluated the grip strength test to examine the muscular strength of rats. As displayed in Fig. 4D, the tMCAO group significantly reduced the average grip score (P < 0.001) in contrast to sham group. However, relative to the tMCAO group, treatment with Rp-S [20 mg/kg b.wt. (P < 0.001)] rapidly increased the average grip score. Similarly, in contradiction to tMCAO group, post-treatment with C-Rp-NPs [10 µg/kg b.wt. (P < 0.001)] elevated the average grip score in a significant manner. However, a non-significant difference in mean grip score was observed at the lowest dose of C-Rp-NPs (1 µg/kg b.wt.).

Finally, the ischemic damage was evaluated by calculating the infarct volume in coronal sections through TTC staining. It is a classic method widely conducted to differentiate metabolically active (red) and inactive tissues (pale). Fig. 4E, F demonstrated significantly higher infarct volumes in the tMCAO group (P < 0.001) compared to the sham group. In contrary to tMCAO group, Rp-S [20 mg/kg b.wt. (P < 0.001)] and C-Rp-NPs [10  $\mu$ g/kg b.wt. (P < 0.001)] considerably reduced the infarct volumes after I/R injury. Consistent with the above results, no discernible decline was found in infarct volumes in rats injected with C-Rp-NPs (1  $\mu$ g/kg b.wt.).

Taken together, our outcomes demonstrated acute neurological dysfunction in tMCAO rodents caused by the neuronal destruction in the motor cortex as evidenced by a lower neuroscore,

grip score, and narrow beam walk test. Nevertheless, improved neurological recovery was observed amongst tMCAO-inflicted rodents following *i.p.* administration of C-Rp-NPs (10 µg/kg b.wt. and 20 µg/kg b.wt.). We, therefore, posited that owing to the abundance of D2 receptors (D2R) in motor regions, *i.e.*, basal ganglia, hence, their stimulation by Rp could be equated with its remedial effectiveness [45]. This D2R expression is further, responsible for mitigating neurological dysfunction *via* minimizing hyperactivity of microglia during I/R injury [46].

Moreover, in the course of I/R injury, injured mitochondrial machinery culminate in mitochondrial-induced apoptotic pathway [47]. This apoptosis leads to the growth of brain infarction along with DNA fragmentation [28]. Furthermore, loss of dopaminergic neurons during I/R injury marked by behavioral deficits could be a consequence of apoptotic cell death [48]. Thus, in the current investigation, the scope of neuronal impairment was estimated by quantifying lesion areas in the cortex region of the brain. Our findings revealed that C-Rp-NPs (10 µg/kg b.wt. and 20 µg/kg b.wt.) attenuated brain infarction in coronal slices of ischemic rodent brain that could be explained with the anti-apoptotic property of Rp [49]. This reduction in infarct volume might inhibit neuronal death that could further reinstate the functional recovery in the C-Rp-NPs injected ischemic rats. It is also worth noting that the C-Rp-NPs were able to reduce the neurological deficits, improve behavioral performances and diminish brain infarctions with similar efficacy even at 1000 times less dose of administrated Rp in contrast to free Rp-S. So, these results are in adherence with C-Rp-NPs ability to target ischemic site in the brain and the technique of the γ-L-Glu-L-Cys homing to ischemic neurons, which is coupled to the over-activation of glutamate receptors of the damaged neurons at the ischemic stroke site [12,50].

#### 3.6. Protective effect of C-Rp-NPs on oxidative stress biomarkers in tMCAO rats

Mitochondrial dysfunction is a major hallmark of ischemic stroke [51]. Besides, reperfusion exacerbates the ischemic state via hampering redox equilibrium in mitochondria thereby, triggering excessive ROS generation [52]. The I/R promoted oxidative stress consequently, contract the contents of defensive antioxidants, increase oxygen intake, promote excess concentrations of iron as well as peroxidisable lipids that function as pro-oxidants and therefore, causes a perturbation in mitochondrial function ultimately leading to cellular death [53]. Rp, however, protects mitochondria from oxidative damage through the diminution of mitochondrial ROS [54]. Accordingly, the anti-oxidant potential of C-Rp-NPs was comprehensively investigated by analyzing the modifications in specific oxidative stress biomarkers such as GSH and LPO spectrophotometrically following tMCAO surgery. Additionally, flow cytometry was utilized in measuring mitochondrial ROS and Δψm. As revealed in Fig. 5A and B, our experimental outcomes showed significantly depleted levels of GSH (P<0.001) and an enhanced LPO rate (calculated as nmoles of thiobarbituric acid reactive substances (TBARS) formed/h/g tissue) (P<0.001) in damaged penumbra tissue of rodents in tMCAO group unlikely to the sham group. Instead, post-treatment with Rp-S [20 mg/kg b.wt. (P<0.001)] and C-Rp-NPs significantly restored the levels of GSH [10 µg/kg b.wt. (P<0.01)and 20  $\mu$ g/kg b.wt. (P<0.001)] and depleted the rate of LPO [1  $\mu$ g/kg b.wt. (P<0.05); 10  $\mu$ g/kg b.wt. (P<0.01) and 20 µg/kg b.wt. (P<0.001)] in damaged penumbra tissue of tMCAOexposed rodents. However, the lowest dose of C-Rp-NPs (1 µg/kg b.wt.) was failed to strive for any notable effect on GSH levels. Further, the production of mitochondrial ROS was estimated by measuring the average fluorescence intensity of ROS-sensitive dye, DCF in

isolated mitochondria. As portrayed in Fig. 5C, D; a significantly high ROS production (P<0.001) was observed in the tMCAO group as opposed to the sham group. On the contrary, post-treatment with Rp-S [20 mg/kg b.wt. (P<0.001)] and C-Rp-NPs significantly scavenged [1  $\mu$ g/kg b.wt. (P<0.001); 10  $\mu$ g/kg b.wt. (P<0.001) and 20  $\mu$ g/kg b.wt. (P<0.001)] ROS in tMCAO rats in a dose-dependent manner.

Disruption in mitochondrial  $\Delta \psi m$  is a primary and chief indicator of mitochondrial dysfunction and subsequently, mitochondrial-mediated apoptosis succeeding I/R injury. Owing to the immoderate build-up of ROS and Ca<sup>2+</sup> in mitochondria, a vicious cascade of mitochondrialinduced apoptotic cell death gets initiated [6]. This in turn leaks cytochrome c from mitochondrial permeability transition pore (mtPTP) into the cytosol, further triggering the activation of downstream caspases. This cascade interrupts the balance of pro-apoptotic and anti-apoptotic proteins thereby, resulting in the loss of neurons by apoptosis [55]. Importantly, the swelling of the mitochondrial matrix caused by the stimulation of mtPTP is responsible for the dissipation of  $\Delta \psi m$  [56]. Therefore, to further explicate the repercussions of mitochondrial ROS production,  $\Delta \psi m$  was measured utilizing TMRE as a probe. The mean TMRE fluorescence intensity showed a substantial reduction (P<0.001) in the tMCAO group in distinction to the sham group which was ultimately retained when treated with Rp-S [20 mg/kg b.wt. (P<0.001)] and C-Rp-NPs [1 µg/kg b.wt. (P<0.001); 10 µg/kg b.wt. (P<0.001) and 20  $\mu$ g/kg b.wt. (P<0.001)] in tMCAO rats in a dose-dependent manner (Fig. 5E, F). This result could be attributed to the binding of doubly charged cationic Rp with negatively charged carboxylate groups of mtPTP at physiological pH by its permeation through the plasma membrane of neuronal cells. Moreover, the lipophilic nature of Rp could be the possible explanation of its binding to both the cytosolic and matrix sides of mtPTP [57]. Henceforward, double-charged cationic and lipophilic property of Rp could reverse mitochondrial swelling and re-establish  $\Delta \psi m$ .

Henceforth, our findings indicated that C-Rp-NPs treatment restored the mitochondrial integrity *via* declining the mitochondrial ROS generation and lipidic oxidation of mitochondrial membranes while increasing the GSH level, thus demonstrating a balance amid oxidant and antioxidant equilibrium of C-Rp-NPs.

## 3.7. Effect of C-Rp-NPs on ATP content in tMCAO rats

Mitochondria generate cellular fuel as ATP. As a consequence of mitochondrial promoted oxidative stress, the redox imbalance and depolarization of the mitochondrial membrane takes place. This results in the alleviation of resperisomal activity (mitochondrial complex enzymes) and eventually disrupts the electron transport chain (ETC) culminating in truncated ATP production [58]. This fact is supported by Fig. 6, wherein a notable decrease (P < 0.001) in ATP content in tMCAO rat's brain tissue was detected compared to the sham group. Interestingly, tMCAO rats injected with Rp-S [20 mg/kg b.wt. (P < 0.001)] and C-Rp-NPs significantly raised [1 µg/kg b.wt. (P < 0.005); 10 µg/kg b.wt. (P < 0.001) and 20 µg/kg b.wt. (P < 0.001)] the ATP content in injured brain tissue.

Our experimental results are in adherence with C-Rp-NPs potential of ameliorating mitochondrial integrity via subduing oxidative stress and reinstating  $\Delta \psi m$  as aforementioned. This might assist in restoring the functions of ETC mitochondrial enzymes and thus, augmenting ATP levels required for neuronal repair mechanisms and their functions [3,59].

Pro-inflammatory cytokines including tumor necrosis factor-alpha (TNF- $\alpha$ ) and interleukin-1 beta (IL-1 $\beta$ ) are considered as contributing factors in oxidative damage and inflammatory reactions coupled with neurodegeneration. Their activation often leads to neuroinflammation and progressive neuronal injuries [60]. Therefore, we assessed the alterations in the expression of TNF- $\alpha$  and IL-1 $\beta$  in the damaged brain tissue. ELISA results disclosed a remarkable increase in TNF- $\alpha$  (P<0.001) and IL-1 $\beta$  (P<0.001) expression in the injured brain of the tMCAO group (Fig. 7A and B) against the sham group. Fascinatingly, lower expression of TNF- $\alpha$  [1 μg/kg b.wt. (P<0.05); 10 μg/kg b.wt. (P<0.01) and 20 μg/kg b.wt. (P<0.001)] and IL-1 $\beta$  [1 μg/kg b.wt. (P<0.001); 10 μg/kg b.wt. (P<0.001) and 20 μg/kg b.wt. (P<0.001)] was seen in the C-Rp-NPs and Rp-S group [20 mg/kg b.wt. (P<0.001)]. These findings are in correlation with the anti-inflammatory property of Rp facilitated by  $\alpha$ B-crystallin and improved cytoplasmic binding action with NF- $\kappa$ B thereby, mitigating neuroinflammation [61].

D2Rs are extensively expressed in the cortex, striatum, and hippocampus regions of the brain. A plethora of reports elaborates on the critical function of D2R expression in dopamineinduced neuroprotection [62]. Previously published results have also documented the decline in D2R expression in the ipsilateral hemisphere during a stroke [63]. It has been very well explained that the D2Rs expression facilitates the modulation of redox reactions and excitotoxicity [62]. Furthermore, up-regulation of D2R stimulates the expression of antiapoptotic protein such as Bcl2 [64]. Also, D2R expression is connected with the management of neuroinflammatory responses and diminish neurological dysfunction by curtailing microglia hyperactivity during I/R injury [46]. Additionally, D2Rs exist in numerous cell types such as endothelium cells for regulating varied functions [65]. Therefore, we further validated the neuroprotective effect of C-Rp-NPs through stimulation of D2Rs in the ischemic brain. ELISA results depicted a significant drop in dopamine levels (P < 0.001) in the tMCAO group contradictorily to the sham group whereas Rp-S [20 mg/kg b.wt. (P<0.001)] and C-Rp-NPs significantly elevated dopamine levels [10  $\mu$ g/kg b.wt. (P<0.01) and 20  $\mu$ g/kg b.wt. (P<0.001)] in the injured brain of tMCAO rats (Fig. 7C). However, the lowest dose of C-Rp-NPs (1 µg/kg b.wt.) was unsuccessful in exerting a significant effect on the expression levels of dopamine in the injured brain tissue. These outcomes were found coinciding with our previous observations mentioned under neurological deficits and behavioral parameters.

## 3.9. Effect of C-Rp-NPs treatment on D2R expression in tMCAO rats

The expression of D2R in the cortical area of the ipsilateral hemisphere was studied by employing immunostaining analysis (Fig. 8A). D2R expression was substantially reduced (P < 0.001) in the tMCAO group than in the sham group. However, post-treatment with Rp-S [20 mg/kg b.wt. (P < 0.001)] and C-Rp-NPs [20 µg/kg b.wt. (P < 0.001)] markedly recovered the D2R expression (shown by brown color) in tMCAO-subjected rats, as evidenced by immunohistochemistry data (Fig. 8B). However, the lowest doses of C-Rp-NPs (1 and 10 µg/kg b.wt.) failed to have a crucial effect on the expression levels of D2R in the ischemic brain tissue. The data, therefore, reinforce the therapeutic potential of C-Rp-NPs through D2R activation following ischemic insult. D2Rs are abundant in the cerebral cortex, striatum, and hippocampus regions of the brain [66]. There is a vast wealth of literature documenting that malfunctioning cortical area induces attention deficits and hyperactivity syndrome [67]. Thus, the outcomes disclosed that I/R injury suppresses D2Rs, leading to the activation of deleterious

signaling pathways, whereas the C-Rp-NPs may confer neuroprotection *via* stimulating D2Rs in the ischemic brain.

3.10. Effects of C-Rp-NPs treatment on Bax/Bcl2 Ratio, cytochrome-c release and Bax translocation in tMCAO rats

Former reports have verified the pivotal role of Bcl2 family-associated proteins [Bcl2, Bcl-xL (also identified as Bcl211), Bax, and Bak1] in the neuronal apoptotic pathway of several neurodegenerative ailments. A pro-apoptotic protein, Bax, is entailed in I/R injury-promoted apoptosis in the brain while Bcl2 being an anti-apoptotic protein is a powerful neuronal-death suppressor [68]. Hence, progression of neuronal injury post-ischemic stroke is highly pronounced by lowered expression of Bcl2 and elevated expression of Bax. Therefore, at last, another vital parameter of therapeutic efficacy *viz.* apoptosis index was tested in tMCAO rats. To this purpose, the ratio of Bax/Bcl2 was estimated which anticipates the apoptotic propensities of neurons. Henceforward, in the tMCAO group, we witnessed significantly higher Bax expression and declined Bcl2 expression (P < 0.001) *versus* the sham group. In addition, Rp-S [20 mg/kg b.wt. (P < 0.001)] and C-Rp-NPs significantly decreased the Bax/Bcl2 ratio [1 µg/kg b.wt. (P < 0.001), 10 µg/kg b.wt. (P < 0.001) and 20 µg/kg b.wt. (P < 0.001)] (Fig. 9A).

We have also inspected the mitochondrial-dependent apoptotic proteins like Bax and cytochrome-c (cyt-c) for further exploration of the neuroprotective mechanism of Rp against I/R injury. It is a well-proven fact that after I/R injury, the translocation of Bax to mitochondria occurs followed by its binding with the outer mitochondrial membrane which increases the mitochondrial permeabilization [69]. This may cause the leakage of cyt-c into the cytoplasm that consequently activates vicious apoptotic cascade and encourages neuronal apoptosis. For this reason, the cytosolic levels of cyt-c were also determined as a marker of mtPTP stimulation and mitochondrial-induced cell death following I/R injury. Thus, as represented in Fig. 9B and C, the brain tissue of tMCAO rats confirmed appreciably greater mitochondrial Bax expression (P<0.001) and lesser cytoplasmic Bax expression (P<0.001) versus sham rats. Contrastingly, mitochondrial as well as cytoplasmic cyt-c levels lowered (P<0.001) and raised (P<0.001), respectively, in the tMCAO group *versus* sham group. These variations conversed *via* treatment with Rp-S [20 mg/kg b.wt. (P<0.001)] and C-Rp-NPs which markedly abrogated the mitochondrial translocation of Bax [1  $\mu$ g/kg b.wt. (P<0.01); 10  $\mu$ g/kg b.wt. (P<0.001) and 20  $\mu$ g/kg b.wt. (P<0.001)] and subsequent release of cyt-c [1  $\mu$ g/kg b.wt. (P<0.001); 10  $\mu$ g/kg b.wt. (P<0.001) and 20 µg/kg b.wt. (P<0.001)] into the cytosol post I/R injury in tMCAO inflicted rats. Our results are, therefore, in sync with previous literature signifying that Rp activates the PI3K/AKT/GSK-3β pathway, which impedes the upregulation and translocation of Bax [7]. Furthermore, Rp is known to reduce the cytoplasmic translocation of cyt-c in most cell lines and in vivo models of Parkinson's disease [49]. Besides, it has also been stated that Rp assembles in mitochondria which is imperative for the effect of such neuroprotectants on mitochondrial channels [70]. Hence, we posited that mechanistic inhibition of cyt-c could be credited to the lessening of mitochondrial Ca<sup>2+</sup> and ROS [6], indirectly as well as a direct impediment of anionic mtPTP through cationic Rp [57].

## 3.11. Effect of C-Rp-NPs on histological deficits in tMCAO rats

The H and E staining method was applied to observe histological modifications in I/R injury to reaffirm the mitochondrial-induced apoptotic suppression at a cellular level by the

administered C-Rp-NPs. As illustrated in Fig. 10A, the frontal cortex region of sham rats displayed no pathological changes and intact neuronal architecture with a readily distinguishable nucleus and cytoplasm. Contradictorily, the vacuolated spaces, pyknotic nuclei, and condensed chromatin in the tMCAO group (P < 0.001) versus the sham group suggested pronounced neurodegeneration as a consequence of necrotic and apoptotic cell death. However, treatment with Rp-S [20 mg/kg b.wt. (P < 0.001)] and C-Rp-NPs [10 µg/kg b.wt. (P < 0.001)] and 20 µg/kg b.wt. (P < 0.001)] effectively resulted in fewer pyknotic nuclei and vacuolation in tMCAO rodents, implying reduced neuronal death in I/R injury (Fig. 10B). Further, the lowest dose of C-Rp-NPs (1 µg/kg b.wt.) had no meaningful influence on neuronal morphology in tMCAO rats. Thus, the findings of the histopathological examinations support our conclusions in the preceding section, wherein we observed an amplified anti-apoptotic impact of C-Rp-NPs as measured by a decrease in the apoptosis index (Bax/Bcl2 ratio).

#### 4. Conclusion

This work accentuated the repurposing of a smart neuroprotectant, ropinirole in Ischemic stroke and Reperfusion Injury and its targeted delivery to the ischemic brain from γ-L-Glu-L-Cys coated HSA nanoformulation via receptor-mediated endocytosis. The fabricated and optimized C-Rp-NPs produced desired drug release and boosted the therapeutic index against I/R injury. Ex vivo confocal microscopy study validated the progressed active homing performance of C-Rp-NPs due to the γ-L-Glu-L-Cys, a potent stimulator of glutamate receptors. Moreover, pharmacokinetics and brain distribution studies revealed that C-Rp-NPs enhanced circulation time in vivo and maintained high therapeutic levels in the brains of Wistar rats upon i.p. administration. Importantly, the C-Rp-NPs can also significantly improve neuroscores, infarct volume, and functional limitations in tMCAO induced I/R injury. The I/R injury therapy experiments indicated that the plausible mechanism behind neuroprotective action of C-Rp-NPs may be mediated via suppression of oxidative stress, pro-inflammatory cytokines, and apoptotic functionality of neurons (3A approach). Furthermore, our findings also specified that C-Rp-NPs treatment significantly ameliorated mitochondrial function via attenuating mitochondrial damage post tMCAO. Also, the chief components of C-Rp-NPs include HSA and ropinirole hydrochloride which have already been approved by US-FDA as well as γ-L-Glu-L-Cys that has gone through clinical trials. Besides, unlike most preclinical investigations that are conducted at initial time-points (preceding to, directly or >3 h after I/R injury), our study was performed at 6 h post-injury, thereby providing a broad window for the treatment and making it more clinically significant. Hence, because of its construction from safe constituents and clinical pertinence of this study, our work thus, provides an innovative and rational tactic for the better treatment of I/R injury based on γ-L-Glu-L-Cys coated Rp loaded HSA NPs and hold great potential for clinical translation.

## **Supporting Information**

Further experimental details, materials, and procedures, including figures and tables of the study, are given in supporting information.

#### **CRediT** author statement

**Saman Fatima:** Conceptualization, Methodology, Formal analysis, Investigation, Resources, Writing - original draft, Funding acquisition. **Mubashshir Ali:** Software, Investigation, Data curation. **Syed Naved Quadri:** Software, Investigation, Data curation. **Sarwar Beg:** Software, Writing - review and editing. **M. Samim:** Supervision, Validation, Visualization, Writing - review and editing. **Suhel Parvez:** Supervision, Conceptualization, Resources. **Malik Zainul** 

**Abdin:** Resources, Visualization, Writing - review and editing. **Prashant Mishra:** Supervision, Conceptualization, Resources. **Farhan Jalees Ahmad:** Supervision, Conceptualization, Resources, Project administration, Funding acquisition.

## **Declaration of competing interest**

The authors declare no competing financial interest.

#### Acknowledgements

This research was generously supported by the Senior Research Fellowship provided to S. Fatima from the Indian Council of Medical Research (ICMR-45/24/2019-NAN-BMS), New Delhi, India. The confocal microscope procured from UGC-SAR (DRS-I) grant by the Department of Biotechnology, SCLS, Jamia Hamdard used in this study is thankfully acknowledged. The authors are also grateful to Dr. Shwetanjali Nimker, BD-JH FACS Academy, BD Biosciences, India for her technical aid in flow cytometry.

#### Data availability

The raw and processed data required to reproduce these findings will be available upon request.

#### References

- (1) S.E. Khoshnam, W. Winlow, M. Farzaneh, Y. Farbood, H.F. Moghaddam, Pathogenic mechanisms following ischemic stroke, Neurol. Sci. 38 (7) (2017) 1167-1186. https://doi.org/10.1007/s10072-017-2938-1.
- (2) S. Fatima, S.N. Quadri, S. Parveen, S. Beg, M.A. Barkat, M. Samim, M.Z. Abdin, F.J. Ahmad, Nanomedicinal strategies as emerging therapeutic avenues to treat and manage cerebral ischemia, CNS Neurol. Disord. Drug Targets 20 (2) (2021) 125-144. https://doi.org/10.2174/1871527319666201102100330.
- (3) P. Kaushik, M. Ali, H. Tabassum, S. Parvez, Post-ischemic administration of dopamine D2 receptor agonist reduces cell death by activating mitochondrial pathway following ischemic stroke, Life Sci. 261 (2020) 118349. <a href="https://doi.org/10.1016/j.lfs.2020.118349">https://doi.org/10.1016/j.lfs.2020.118349</a>.
- (4) S.S. Andrabi, S. Parvez, H. Tabassum, Progesterone induces neuroprotection following reperfusion-promoted mitochondrial dysfunction after focal cerebral ischemia in rats, Dis. Model. Mech. 10 (6) (2017) 787-796. <a href="https://doi.org/10.1242/dmm.025692">https://doi.org/10.1242/dmm.025692</a>.
- (5) L. Gong, Y. Tang, R. An, M. Lin, L. Chen, J. Du, RTN1-C mediates cerebral ischemia/reperfusion injury via ER stress and mitochondria-associated apoptosis pathways, Cell Death Dis. 8 (10) (2017) e3080. <a href="https://doi.org/10.1038/cddis.2017.465">https://doi.org/10.1038/cddis.2017.465</a>.
- (6) S.S. Andrabi, H. Tabassum, S. Parveen, S. Parvez, Ropinirole induces neuroprotection following reperfusion-promoted mitochondrial dysfunction after focal cerebral ischemia in Wistar rats, Neurotoxicology 77 (2020) 94-104. <a href="https://doi.org/10.1016/j.neuro.2019.12.004">https://doi.org/10.1016/j.neuro.2019.12.004</a>.
- (7) S. Chen, X. Zhang, D. Yang, Y. Du, L. Li, X. Li, M. Ming, W. Le, D2/D3 receptor agonist ropinirole protects dopaminergic cell line against rotenone-induced apoptosis through inhibition of caspase-and JNK-dependent pathways, FEBS Lett. 582 (5) (2008) 603-610. <a href="https://doi.org/10.1016/j.febslet.2008.01.028">https://doi.org/10.1016/j.febslet.2008.01.028</a>.

- (8) V.D. Nair, C.W. Olanow, Differential modulation of Akt/glycogen synthase kinase-3β pathway regulates apoptotic and cytoprotective signaling responses, J. Biol. Chem. 283 (22) (2008) 15469-15478. https://doi.org/10.1074/jbc.M707238200.
- (9) C.M. Kaye, B. Nicholls, Clinical pharmacokinetics of ropinirole, Clin. Pharmacokinet. 39 (4) (2000) 243-254. <a href="https://doi.org/10.2165/00003088-200039040-00001">https://doi.org/10.2165/00003088-200039040-00001</a>.
- (10) D. Pradhan, V. Tambe, N. Raval, P. Gondalia, P. Bhattacharya, K. Kalia, R.K. Tekade, Dendrimer grafted albumin nanoparticles for the treatment of post cerebral stroke damages: A proof of concept study, Colloids Surf. B Biointerfaces 184 (2019) 110488. https://doi.org/10.1016/j.colsurfb.2019.110488.
- (11) F. Kratz, A clinical update of using albumin as a drug vehicle—A commentary, J. Control. Release 190 (2014) 331-336. https://doi.org/10.1016/j.jconrel.2014.03.013.
- (12) S. Fatima, T. Mohammad, D.S. Jairajpuri, M.T. Rehman, A. Hussain, M. Samim, F.J. Ahmad, M.F. Alajmi, M.I. Hassan, Identification and evaluation of glutathione conjugate gamma-l-glutamyl-l-cysteine for improved drug delivery to the brain, J. Biomol. Struct. Dyn. 38 (12) (2020) 3610-3620. https://doi.org/10.1080/07391102.2019.1664937.
- (13) H. Nosrati, M. Tarantash, S. Bochani, J. Charmi, Z. Bagheri, M. Fridoni, M.A. Abdollahifar, S. Davaran, H. Danafar, H. Kheiri Manjili, Glutathione (GSH) peptide conjugated magnetic nanoparticles as blood—brain barrier shuttle for MRI-monitored brain delivery of paclitaxel, ACS Biomater. Sci. Eng. 5 (4) (2019) 1677-1685. <a href="https://doi.org/10.1021/acsbiomaterials.8b01420">https://doi.org/10.1021/acsbiomaterials.8b01420</a>.
- (14) A. Jahanban-Esfahlan, S. Dastmalchi, S. Davaran, A simple improved desolvation method for the rapid preparation of albumin nanoparticles, Int. J. Biol. Macromol. 91 (2016) 703-709. https://doi.org/10.1016/j.ijbiomac.2016.05.032.
- (15) S. Fatima, S. Beg, M. Samim, F.J. Ahmad, Application of chemometric approach for development and validation of high performance liquid chromatography method for estimation of ropinirole hydrochloride, J. Sep. Sci. 42 (21) (2019) 3293-3301. <a href="https://doi.org/10.1002/jssc.201900458">https://doi.org/10.1002/jssc.201900458</a>.
- (16) Y. Shen, W. Li, HA/HSA co-modified erlotinib—albumin nanoparticles for lung cancer treatment, Drug Des. Devel. Ther. 12 (2018) 2285-2292. <a href="https://doi.org/10.2147/DDDT.S169734">https://doi.org/10.2147/DDDT.S169734</a>.
- (17) S. Ahmed, A. Gull, M. Aqil, M.D. Ansari, Y. Sultana, Poloxamer-407 thickened lipid colloidal system of agomelatine for brain targeting: Characterization, brain pharmacokinetic study and behavioral study on Wistar rats, Colloids Surf. B Biointerfaces 181 (2019) 426-436. <a href="https://doi.org/10.1016/j.colsurfb.2019.05.016">https://doi.org/10.1016/j.colsurfb.2019.05.016</a>.
- (18) B. Wilson, M.K. Samanta, K. Santhi, K.P. Kumar, N. Paramakrishnan, B. Suresh, Targeted delivery of tacrine into the brain with polysorbate 80-coated poly (n-butylcyanoacrylate) nanoparticles, Eur. J. Pharm. Biopharm. 70 (1) (2008) 75-84. https://doi.org/10.1016/j.ejpb.2008.03.009.

- (19) L.A. De Girolamo, A.J. Hargreaves, E.E. Billett, Protection from MPTP-induced neurotoxicity in differentiating mouse N2a neuroblastoma cells, J. Neurochem. 76 (3) (2001) 650-660. <a href="https://doi.org/10.1046/j.1471-4159.2001.00066.x">https://doi.org/10.1046/j.1471-4159.2001.00066.x</a>.
- (20) A. Arora, S. Kumar, J. Ali, S. Baboota, Intranasal delivery of tetrabenazine nanoemulsion via olfactory region for better treatment of hyperkinetic movement associated with Huntington's disease: Pharmacokinetic and brain delivery study, Chem. Phys. Lipids 230 (2020) 104917. https://doi.org/10.1016/j.chemphyslip.2020.104917.
- (21) X. Liu, C. An, P. Jin, X. Liu, L. Wang, Protective effects of cationic bovine serum albumin-conjugated PEGylated tanshinone IIA nanoparticles on cerebral ischemia, Biomaterials 34 (3) (2013) 817-830. https://doi.org/10.1016/j.biomaterials.2012.10.017.
- (22) S.W. Kang, B. Seo, J.H. Kim, O.K. Kim, J.H. Shin, G.J. Lee, H.K. Park, Cell viability, adhesion and function of RAW 264.7 macrophages on fluorinated xerogel-derived nitric oxide permeable membrane for the application of cellular sensing, J. Nanosci. Nanotechnol. 14 (11) (2014) 8398-8404. https://doi.org/10.1166/jnn.2014.9928.
- (23) J.B. Bederson, L.H. Pitts, M. Tsuji, M.C. Nishimura, R.L. Davis, H.E. Bartkowski, Rat middle cerebral artery occlusion: evaluation of the model and development of a neurologic examination, Stroke 17 (3) (1986) 472-476. https://doi.org/10.1161/01.STR.17.3.472.
- (24) H. Bai, L. Zhao, H. Liu, H. Guo, W. Guo, L. Zheng, X. Liu, X. Wu, J. Luo, X. Li, L. Gao, Adiponectin confers neuroprotection against cerebral ischemia-reperfusion injury through activating the cAMP/PKA-CREB-BDNF signaling, Brain Res. Bull. 143 (2018) 145-154. <a href="https://doi.org/10.1016/j.brainresbull.2018.10.013">https://doi.org/10.1016/j.brainresbull.2018.10.013</a>.
- (25) S. Chaudhary, S. Parvez, An in vitro approach to assess the neurotoxicity of valproic acid-induced oxidative stress in cerebellum and cerebral cortex of young rats, Neuroscience 225 (2012) 258-268. https://doi.org/10.1016/j.neuroscience.2012.08.060.
- (26) M. Ashafaq, H. Tabassum, S. Parvez, Modulation of behavioral deficits and neurodegeneration by tannic acid in experimental stroke challenged Wistar rats, Mol. Neurobiol. 54 (8) (2017) 5941-5951. https://doi.org/10.1007/s12035-016-0096-8.
- (27) T.H. Sanderson, G. Mahapatra, P. Pecina, Q. Ji, K. Yu, C. Sinkler, A. Varughese, R. Kumar, M.J. Bukowski, R.N. Tousignant, A.R. Salomon, I. Lee, M. Hüttemann, Cytochrome c is tyrosine 97 phosphorylated by neuroprotective insulin treatment, PLoS One 8 (11) (2013) e78627. https://doi.org/10.1371/journal.pone.0078627.
- (28) P. Wicha, J. Tocharus, A. Janyou, J. Jittiwat, C. Changtam, A. Suksamrarn, C. Tocharus, Hexahydrocurcumin protects against cerebral ischemia/reperfusion injury, attenuates inflammation, and improves antioxidant defenses in a rat stroke model, PloS One 12 (12) (2017) e0189211. https://doi.org/10.1371/journal.pone.0189211.
- (29) G.V. Patil, Biopolymer albumin for diagnosis and in drug delivery, Drug Dev. Res. 58 (3) (2003) 219-247. https://doi.org/10.1002/ddr.10157.

- (30) K. Langer, S. Balthasar, V. Vogel, N. Dinauer, H. Von Briesen, D. Schubert, Optimization of the preparation process for human serum albumin (HSA) nanoparticles, Int. J. Pharm. 257 (1-2) (2003) 169-180. https://doi.org/10.1016/S0378-5173(03)00134-0.
- (31) A.O. Elzoghby, W.M. Samy, N.A. Elgindy, Albumin-based nanoparticles as potential controlled release drug delivery systems, J. Control. Release 157 (2) (2012) 168-182. <a href="https://doi.org/10.1016/j.jconrel.2011.07.031">https://doi.org/10.1016/j.jconrel.2011.07.031</a>.
- (32) N. Raval, P. Barai, N. Acharya, S. Acharya, Fabrication of peptide-linked albumin nanoconstructs for receptor-mediated delivery of asiatic acid to the brain as a preventive measure in cognitive impairment: optimization, in-vitro and in-vivo evaluation, Artif. Cells Nanomed. Biotechnol. 46 (sup3) (2018) S832-S846. <a href="https://doi.org/10.1080/21691401.2018.1513942">https://doi.org/10.1080/21691401.2018.1513942</a>.
- (33) M.I. Alam, S. Baboota, A. Ahuja, M. Ali, J. Ali, J.K. Sahni, Nanostructured lipid carrier containing CNS acting drug: formulation, optimization and evaluation, Curr. Nanosci. 7 (6) (2011) 1014-1027. <a href="https://doi.org/10.2174/1573413711107061014">https://doi.org/10.2174/1573413711107061014</a>.
- (34) C. Saraiva, C. Praça, R. Ferreira, T. Santos, L. Ferreira, L. Bernardino, Nanoparticle-mediated brain drug delivery: overcoming blood—brain barrier to treat neurodegenerative diseases, J. Control. Release 235 (2016) 34-47. <a href="https://doi.org/10.1016/j.jconrel.2016.05.044">https://doi.org/10.1016/j.jconrel.2016.05.044</a>.
- (35) B. Wilson, Y. Lavanya, S.R. Priyadarshini, M. Ramasamy, J.L. Jenita, Albumin nanoparticles for the delivery of gabapentin: preparation, characterization and pharmacodynamic studies, Int. J. Pharm. 473 (1-2) (2014) 73-79. https://doi.org/10.1016/j.ijpharm.2014.05.056.
- (36) X. Guo, G. Deng, J. Liu, P. Zou, F. Du, F. Liu, A.T. Chen, R. Hu, M. Li, S. Zhang, Z. Tang, Thrombin-responsive, brain-targeting nanoparticles for improved stroke therapy, ACS Nano 12 (8) (2018) 8723-8732. https://doi.org/10.1021/acsnano.8b04787.
- (37) K.T. LePage, R.W. Dickey, W.H. Gerwick, E.L. Jester, T.F. Murray, On the use of neuro-2a neuroblastoma cells versus intact neurons in primary culture for neurotoxicity studies, Crit. Rev. Neurobiol. 17 (1) (2005) 27-50. https://doi.org/10.1615/critrevneurobiol.v17.i1.20.
- (38) Y. Kang, Z. Wu, D. Cai, B. Lu, Evaluation of reference genes for gene expression studies in mouse and N2a cell ischemic stroke models using quantitative real-time PCR, BMC Neurosci. 19 (1) (2018) 1-11. <a href="https://doi.org/10.1186/s12868-018-0403-6">https://doi.org/10.1186/s12868-018-0403-6</a>.
- (39) P. Provost, Interpretation and applicability of microRNA data to the context of Alzheimer's and age-related diseases, Aging 2 (3) (2010) 166-169. https://doi.org/10.18632/aging.100131.
- (40) R. Salto, J.D. Vílchez, M.D. Girón, E. Cabrera, N. Campos, M. Manzano, R. Rueda, J.M. López-Pedrosa, β-Hydroxy-β-methylbutyrate (HMB) promotes neurite outgrowth in Neuro2a cells, PloS One 10 (8) (2015) e0135614. https://doi.org/10.1371/journal.pone.0135614.
- (41) P.V. Turner, T. Brabb, C. Pekow, M.A. Vasbinder, Administration of substances to laboratory animals: routes of administration and factors to consider, J. Am. Assoc. Lab. Anim. Sci. 50 (5) (2011) 600-613.

- (42) F.F. An, X.H. Zhang, Strategies for preparing albumin-based nanoparticles for multifunctional bioimaging and drug delivery, Theranostics 7 (15) (2017) 3667-3689. https://doi.org/10.7150/thno.19365.
- (43) K. Maruyama, N. Takahashi, T. Tagawa, K. Nagaike, M. Iwatsuru, Immunoliposomes bearing polyethyleneglycol-coupled Fab' fragment show prolonged circulation time and high extravasation into targeted solid tumors in vivo, FEBS Lett. 413 (1) (1997) 177-180. <a href="https://doi.org/10.1016/S0014-5793(97)00905-8">https://doi.org/10.1016/S0014-5793(97)00905-8</a>.
- (44) M. Balkaya, J.M. Krober, A. Rex, M. Endres, Assessing post-stroke behavior in mouse models of focal ischemia, J. Cereb. Blood Flow Metab. 33 (3) (2013) 330–338. https://doi.org/10.1038/jcbfm.2012.185.
- (45) C. Yang, J.R. Zhang, L. Chen, S.N. Ge, J.L. Wang, Z.Q. Yan, D. Jia, J.L. Zhu, G.D. Gao, Decreased HCN2 expression in STN contributes to abnormal high-voltage spindles in the cortex and globus pallidus of freely moving rats, Brain Res. 1618 (2015) 17-28. https://doi.org/10.1016/j.brainres.2015.05.009.
- (46) C.H. Gil, Y.R. Kim, H.J. Lee, D.H. Jung, H.K. Shin, B.T. Choi, Aripiprazole exerts a neuroprotective effect in mouse focal cerebral ischemia, Exp. Ther. Med. 15 (1) (2017) 745-750. <a href="https://doi.org/10.3892/etm.2017.5443">https://doi.org/10.3892/etm.2017.5443</a>.
- (47) K. Todd, J. Ghiso, A. Rostagno, Oxidative stress and mitochondria-mediated cell death mechanisms triggered by the familial Danish dementia ADan amyloid, Neurobiol. Dis. 85 (2016) 130-143. <a href="https://doi.org/10.1016/j.nbd.2015.10.003">https://doi.org/10.1016/j.nbd.2015.10.003</a>.
- (48) Z.F. Zhong, J. Han, J.Z. Zhang, Q. Xiao, J.Y. Chen, K. Zhang, J. Hu, L.D. Chen, Neuroprotective effects of salidroside on cerebral ischemia/reperfusion-induced behavioral impairment involves the dopaminergic system, Front. Pharmacol. 10 (2019) 1433. https://doi.org/10.3389/fphar.2019.01433.
- (49) G. Park, Y.J. Park, H.O. Yang, M.S. Oh, Ropinirole protects against 1-methyl-4-phenyl-1, 2, 3, 6-tetrahydropyridine (MPTP)-induced neurotoxicity in mice via anti-apoptotic mechanism, Pharmacol. Biochem. Behav. 104 (2013) 163-168. <a href="https://doi.org/10.1016/j.pbb.2013.01.017">https://doi.org/10.1016/j.pbb.2013.01.017</a>.
- (50) W. Lv, J. Xu, X. Wang, X. Li, Q. Xu, H. Xin, Bioengineered boronic ester modified dextran polymer nanoparticles as reactive oxygen species responsive nanocarrier for ischemic stroke treatment, ACS Nano 12 (6) (2018) 5417-5426. https://doi.org/10.1021/acsnano.8b00477.
- (51) W.S. Gibbs, R.A. Weber, R.G. Schnellmann, D.L. Adkins, Disrupted mitochondrial genes and inflammation following stroke, Life Sci. 166 (2016) 139-148. <a href="https://doi.org/10.1016/j.lfs.2016.09.021">https://doi.org/10.1016/j.lfs.2016.09.021</a>.
- (52) Y.X. Zhao, M. Cui, S.F. Chen, Q. Dong, X.Y. Liu, Amelioration of ischemic mitochondrial injury and Bax-dependent outer membrane permeabilization by Mdivi-1, CNS Neurosci. Ther. 20 (6) (2014) 528-538. https://doi.org/10.1111/cns.12266.
- (53) H. Bayir, V.E. Kagan, Bench-to-bedside review: Mitochondrial injury, oxidative stress and apoptosis—there is nothing more practical than a good theory, Crit. Care 12 (1) (2008) 206. <a href="https://doi.org/10.1186/cc6779">https://doi.org/10.1186/cc6779</a>.

- (54) K.S. Chahal, A. Prakash, A.B. Majeed, The role of multifunctional drug therapy against carbamate induced neuronal toxicity during acute and chronic phase in rats, Environ. Toxicol. Pharmacol. 40 (1) (2015) 220-229. https://doi.org/10.1016/j.etap.2015.06.002.
- (55) O.V. Akopova, L.I. Kolchinskaya, V.I. Nosar, V.A. Bouryi, I.N. Mankovska, V.F. Sagach, Cytochrome C as an amplifier of ROS release in mitochondria, Fiziol Zh. 58 (1) (2012) 3-12.
- (56) R. Wong, C. Steenbergen, E. Murphy, Mitochondrial permeability transition pore and calcium handling, Methods Mol. Biol. 810 (2012) 235-242. <a href="https://doi.org/10.1007/978-1-61779-382-0\_15">https://doi.org/10.1007/978-1-61779-382-0\_15</a>.
- (57) S. Parvez, K. Winkler-Stuck, S. Hertel, P. Schönfeld, D. Siemen, The dopamine-D2-receptor agonist ropinirole dose-dependently blocks the Ca<sup>2+</sup>-triggered permeability transition of mitochondria, Biochim. Biophys. Acta 1797 (6-7) (2010) 1245-1250. <a href="https://doi.org/10.1016/j.bbabio.2010.02.001">https://doi.org/10.1016/j.bbabio.2010.02.001</a>.
- (58) J.V. Leonard, A.H. Schapira, Mitochondrial respiratory chain disorders II: neurodegenerative disorders and nuclear gene defects, Lancet. 355 (9201) (2000) 389-394. https://doi.org/10.1016/S0140-6736(99)05226-5.
- (59) J. Chen, L. Wang, C. Wu, Q. Hu, C. Gu, F. Yan, J. Li, W. Yan, G. Chen, Melatonin-enhanced autophagy protects against neural apoptosis via a mitochondrial pathway in early brain injury following a subarachnoid hemorrhage, J. Pineal Res. 56 (1) (2014) 12-19. https://doi.org/10.1111/jpi.12086.
- (60) K.S. Kirkley, K.A. Popichak, M.F. Afzali, M.E. Legare, R.B. Tjalkens, Microglia amplify inflammatory activation of astrocytes in manganese neurotoxicity, J. Neuroinflammation 14 (1) (2017) 99. <a href="https://doi.org/10.1186/s12974-017-0871-0">https://doi.org/10.1186/s12974-017-0871-0</a>.
- (61) Y. Zhang, Y. Chen, J. Wu, A. Manaenko, P. Yang, J. Tang, W. Fu, J.H. Zhang, Activation of dopamine D2 receptor suppresses neuroinflammation through αB-crystalline by inhibition of NF-κB nuclear translocation in experimental ICH mice model, Stroke 46 (9) (2015) 2637-2646. https://doi.org/10.1161/STROKEAHA.115.009792.
- (62) Y. Bozzi, E. Borrelli, Dopamine in neurotoxicity and neuroprotection: what do D2 receptors have to do with it? Trends Neurosci. 29 (3) (2006) 167-174. <a href="https://doi.org/10.1016/j.tins.2006.01.002">https://doi.org/10.1016/j.tins.2006.01.002</a>.
- (63) A. Gower, M. Tiberi, The intersection of central dopamine system and stroke: potential avenues aiming at enhancement of motor recovery, Front. Synaptic Neurosci. 10 (2018) 18. <a href="https://doi.org/10.3389/fnsyn.2018.00018">https://doi.org/10.3389/fnsyn.2018.00018</a>.
- (64) T. Kihara, S. Shimohama, H. Sawada, K. Honda, T. Nakamizo, R. Kanki, H. Yamashita, A. Akaike, Protective effect of dopamine D2 agonists in cortical neurons via the phosphatidylinositol 3 kinase cascade, J. Neurosci. Res. 70 (3) (2002) 274-282. https://doi.org/10.1002/jnr.10426.
- (65) A.V. Andjelkovic, J. Xiang, S.M. Stamatovic, Y. Hua, G. Xi, M.M. Wang, R.F. Keep, Endothelial targets in stroke: translating animal models to human, Arterioscler. Thromb. Vasc. Biol. 39 (11) (2019) 2240-2247. https://doi.org/10.1161/ATVBAHA.119.312816.

- (66) X. Wei, T. Ma, Y. Cheng, C.C. Huang, X. Wang, J. Lu, J. Wang, Dopamine D1 or D2 receptor-expressing neurons in the central nervous system, Addict. Biol. 23 (2) (2018) 569-584. https://doi.org/10.1111/adb.12512.
- (67) C. Sarkar, B. Basu, D. Chakroborty, P.S. Dasgupta, S. Basu, The immunoregulatory role of dopamine: an update, Brain Behav. Immun. 24 (4) (2010) 525–528. https://doi.org/10.1016/j.bbi.2009.10.015.
- (68) E.A. Jonas, G.A. Porter, K.N. Alavian, Bcl-xL in neuroprotection and plasticity, Front. Physiol. 5 (2014) 355. <a href="https://doi.org/10.3389/fphys.2014.00355">https://doi.org/10.3389/fphys.2014.00355</a>.
- (69) R.F. Gahl, P. Dwivedi, N. Tjandra, Bcl-2 proteins bid and bax form a network to permeabilize the mitochondria at the onset of apoptosis, Cell Death Dis. 7 (10) (2016) e2424. https://doi.org/10.1038/cddis.2016.320.
- (70) R. Danzeisen, B. Schwalenstoecker, F. Gillardon, E. Buerger, V. Krzykalla, K. Klinder, L. Schild, B. Hengerer, A.C. Ludolph, C. Dorner-Ciossek, L. Kussmaul, Targeted antioxidative and neuroprotective properties of the dopamine agonist pramipexole and its nondopaminergic enantiomer SND919CL2x [(+) 2-amino-4, 5, 6, 7-tetrahydro-6-Lpropylamino-benzathiazole dihydrochloride], J. Pharmacol. Exp. Ther. 316 (1) (2006) 189-199. <a href="https://doi.org/10.1124/jpet.105.092312">https://doi.org/10.1124/jpet.105.092312</a>.

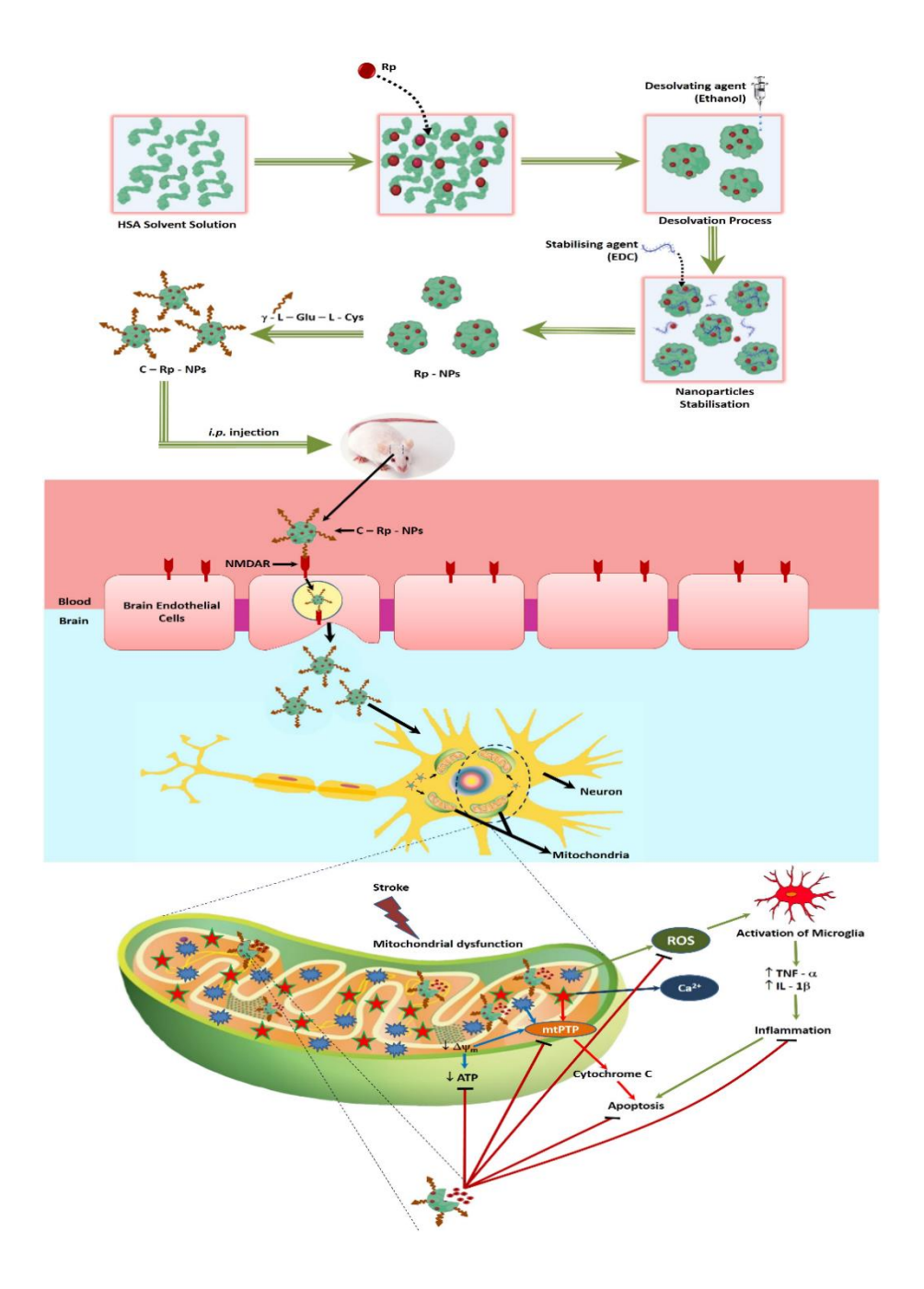


**Fig. 1.** Brain-targeted delivery of  $\gamma$ -L-Glu-L-Cys layered ropinirole-entrapped HSA nanoparticles (C-Rp-NPs) for effective protection against I/R injury. C-Rp-NPs are fabricated by taking advantage of the widely acknowledged desolvation technique followed by layering of  $\gamma$ -L-Glu-L-Cys on the surface of Rp-NPs through physical adsorption. Following intraperitoneal administration, C-Rp-NPs accumulate in the ischemic neurons *via* exploiting the high intrinsic affinity between  $\gamma$ -L-Glu-L-Cys and locally overexpressed glutamate receptors (NMDA and AMPA). Afterward, the C-Rp-NPs are taken up by the mitochondria thereby, triggering the mitochondrial-mediated neuroprotection through inhibition of the toxic reactive oxygen species production and secretion of pro-inflammatory cytokines, thus, attenuating oxidative stress and neuroinflammation. Further, C-Rp-NPs supplementation also impedes the expression of apoptosis-allied proteins hence, mitigating tMCAO-induced neuronal apoptosis and alleviating the advancement of I/R injury.

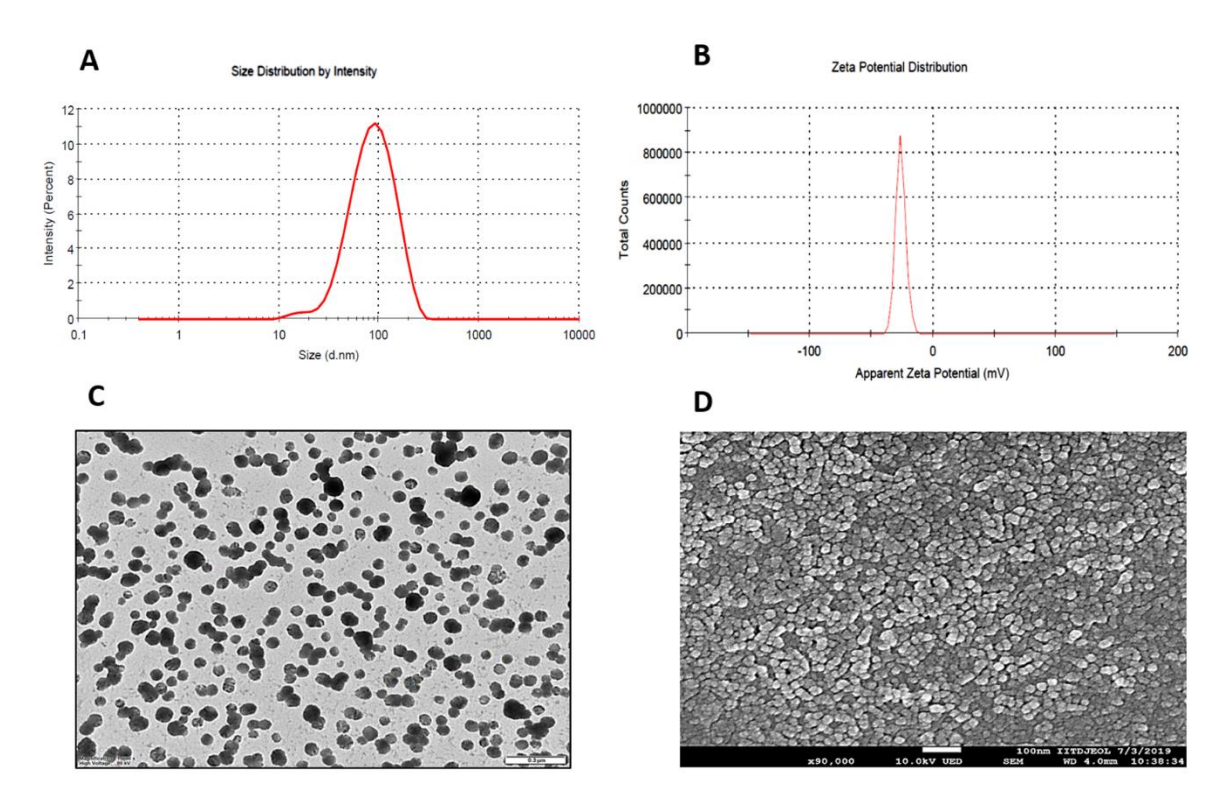


**Fig. 2.** Characterization of C-Rp-NPs. (A) Particle size and size distribution. (B) Surface charge. Morphological examination of C-Rp-NPs using; (C) TEM and (D) FESEM. Sphere-shaped particles with smooth surfaces as well as smaller particles of size  $\leq 100$  nm were apparent, which is favorable for its transport across the blood-brain barrier (BBB).

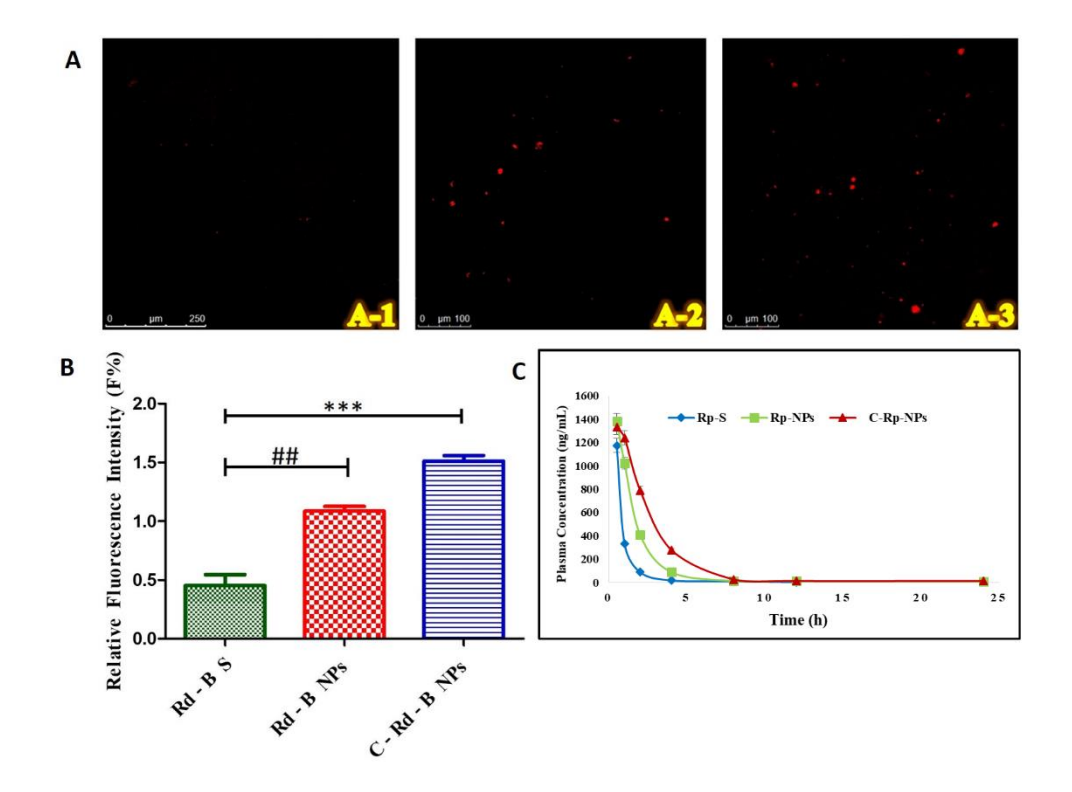


**Fig. 3.** Confocal Microscopy showing trafficking profile of different nanoparticles loaded with Rd-B dye in the brain, comprising (A-1) Rd-B S, (A-2) Rd-B NPs, and (A-3) C-Rd-B NPs. (B) The percentage of relative fluorescence intensity in coronal slices of the brain exhibited by Rd-B S, Rd-B NPs, and C-Rd-B NPs. Data in B are represented as means  $\pm$  SEM (n = 3 per group). ##P < 0.01, Rd-B S vs. Rd-B NPs and \*\*\*P < 0.001, Rd-B S vs. C-Rd-B NPs (one-way ANOVA with Tukey's multiple comparisons test). (C) *In vivo* pharmacokinetics of free Rp-S, Rp-NPs, and C-Rp-NPs. Data in C are represented as means  $\pm$  SD (n = 3 per time point).

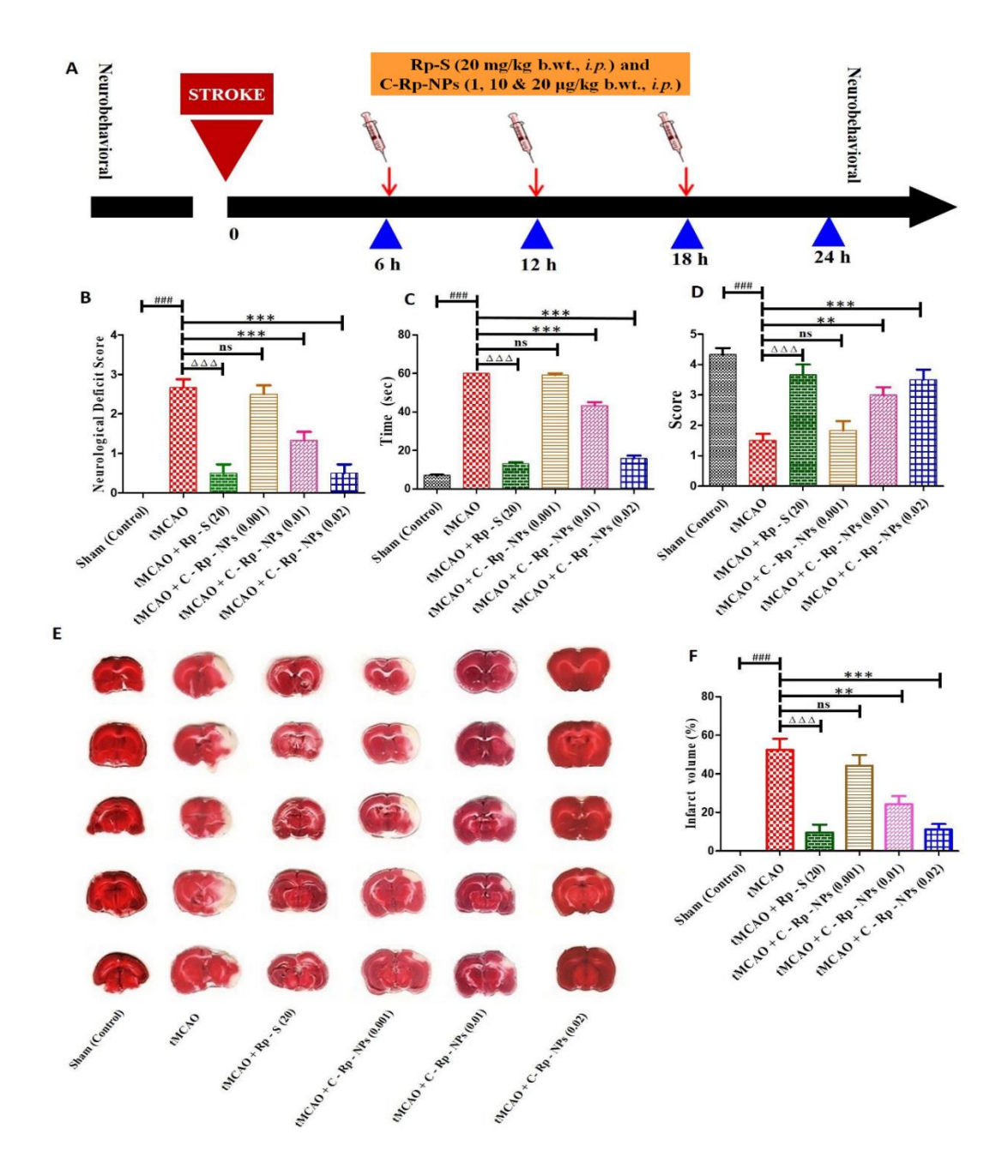


**Fig. 4.** C-Rp-NPs administration ameliorates neurobehavioural impairments and reduces neuronal injury in ischemic rats. (A) An outline of experimental paradigm. (B) Neurological Deficit Score. (C) Narrow Beam Walk Test. (D) Grip Strength Score. Data in B, C and D are represented as means  $\pm$  SEM (n = 6 per group). \*\*#\*P < 0.001, Sham vs. tMCAO; \*\* $\Delta \Delta \Delta \Delta P < 0.001$ , tMCAO+Rp-S (20) vs. tMCAO; \*\* $\Delta \Delta \Delta P = 0.001$ , tMCAO+C-Rp-NPs (0.01) vs. tMCAO and \*\*\* $\Delta \Delta P = 0.001$ , tMCAO+C-Rp-NPs (0.02) vs. tMCAO (one-way ANOVA with Tukey's multiple comparisons test). Diminishing effect of C-Rp-NPs on infarct volume of ischemic brains in rats: (E) Evaluation of TTC stained coronal brain sections of tMCAO, Rp-S and C-Rp-NPs treated rats, (F) Quantification of Infarct Volumes. Data in F are represented as means  $\pm$  SEM (n = 3 per group). \*\*#\* $\Delta \Delta \Delta P = 0.001$ , Sham vs. tMCAO; \*\* $\Delta \Delta \Delta P = 0.001$ , tMCAO+Rp-S (20) vs. tMCAO; \*\* $\Delta \Delta P = 0.001$ , tMCAO+C-Rp-NPs (0.01) vs. tMCAO and \*\*\*\* $\Delta P = 0.001$ , tMCAO+C-Rp-NPs (0.01) vs. tMCAO and \*\*\*\* $\Delta P = 0.001$ , tMCAO+C-Rp-NPs (0.01) vs. tMCAO and \*\*\*\* $\Delta P = 0.001$ , tMCAO+C-Rp-NPs (0.01) vs. tMCAO (one-way ANOVA with Tukey's multiple comparisons test).

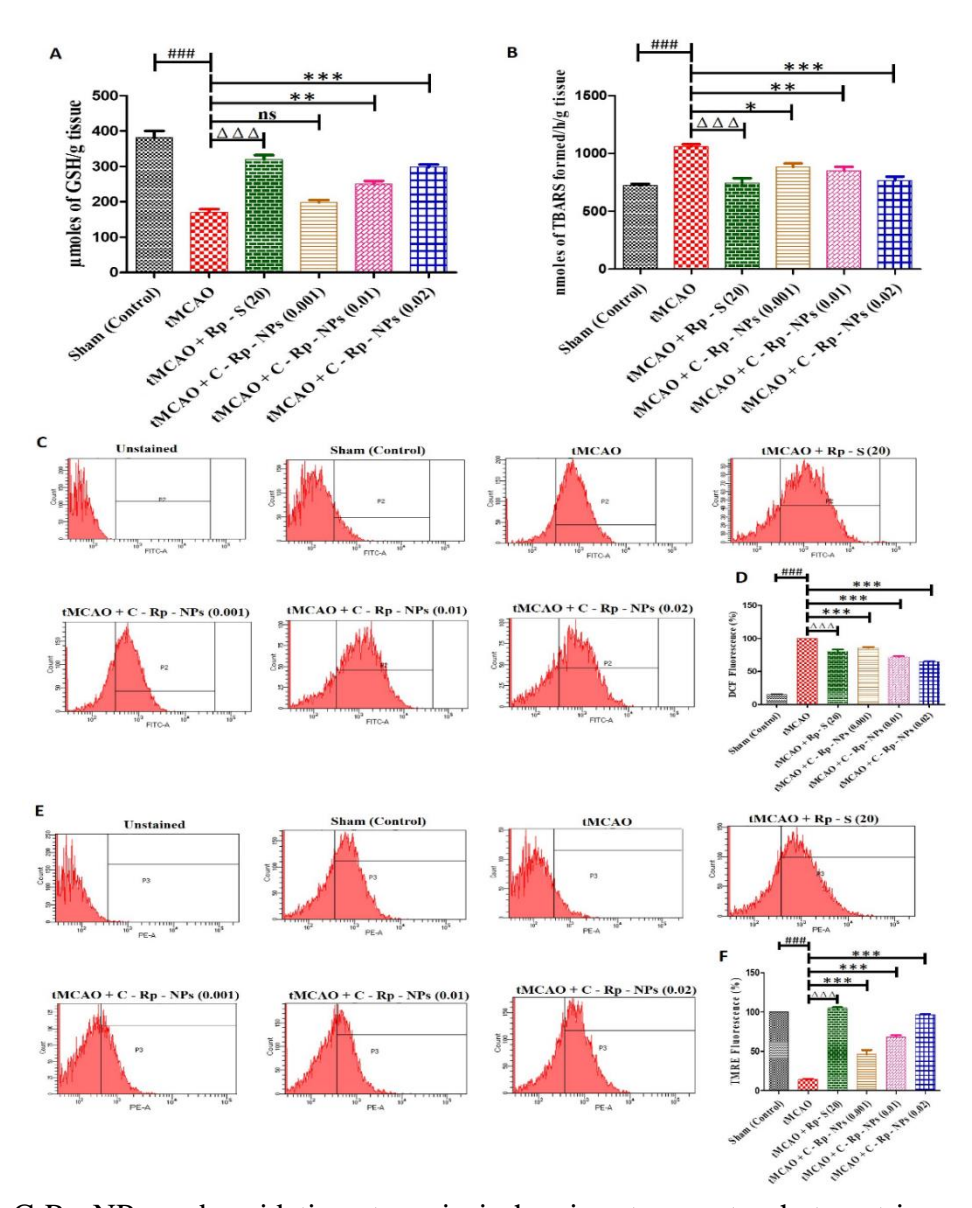
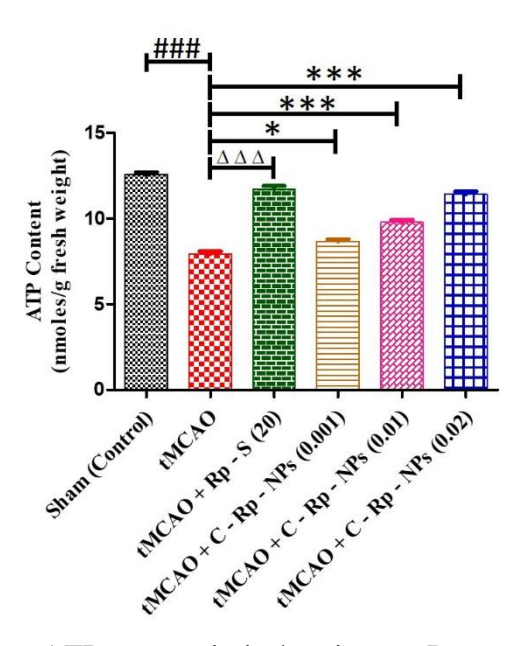
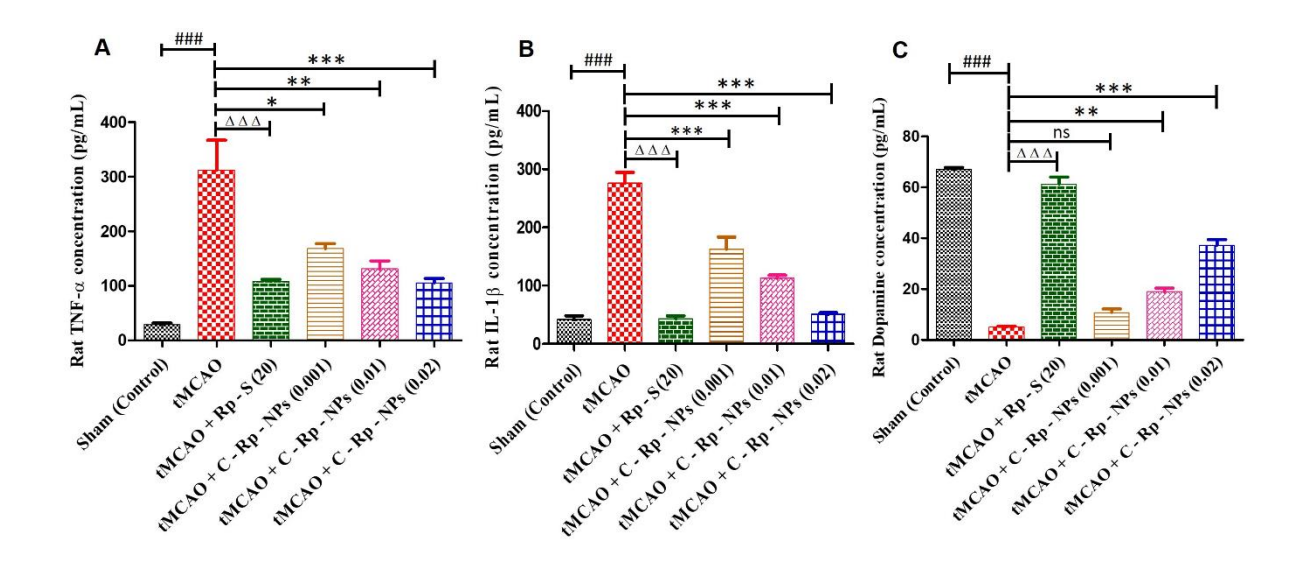


Fig. 5. C-Rp-NPs curb oxidative stress in ischemic rats: spectrophotometric exploration of oxidative stress biomarkers (A) GSH (B) LPO. Data in A and B are represented as means ± SEM (n = 3 per group). \*##P < 0.001, Sham vs. tMCAO;  $\triangle AAAP < 0.001$ , tMCAO+Rp-S (20) vs. tMCAO;  $^{ns}P$  = not significant;  $^*P < 0.05$ , tMCAO+C-Rp-NPs (0.001) vs. tMCAO;  $^{**}P < 0.01$ , tMCAO+C-Rp-NPs (0.01) vs. tMCAO and \*\*\*P < 0.001, tMCAO+C-Rp-NPs (0.02) vs. tMCAO (one-way ANOVA with Tukey's multiple comparisons test). C-Rp-NPs administration inhibit mitochondrial ROS generation. (C) DCF fluorescence in mitochondria in sham, tMCAO, tMCAO+Rp-S (20), tMCAO+C-Rp-NPs (0.001), tMCAO+C-Rp-NPs (0.01) and tMCAO+C-Rp-NPs (0.02) groups. (D) Mean fluorescence intensity. C-Rp-NPs administration modulate membrane potential of mitochondria. (E) TMRE fluorescence in mitochondria in sham, tMCAO, tMCAO+Rp-S (20), tMCAO+C-Rp-NPs (0.001), tMCAO+C-Rp-NPs (0.01) and tMCAO+C-Rp-NPs (0.02) groups. (F) Mean fluorescence intensity. Data in D and F are represented as means  $\pm$  SEM (n = 3 per group). ###P < 0.001, Sham vs. tMCAO;  $^{44A}P < 0.001$ , tMCAO+Rp-S (20) vs. tMCAO; \*\*\* P < 0.001, tMCAO+C-Rp-NPs (0.001) vs. tMCAO; \*\*\*P < 0.001, tMCAO+C-Rp-NPs (0.01) vs. tMCAO and \*\*\*P < 0.001, tMCAO+C-Rp-NPs (0.02) vs. tMCAO (one-way ANOVA with Tukey's multiple comparisons test).



**Fig. 6.** C-Rp-NPs elevate ATP content in ischemic rats. Data are represented as means  $\pm$  SEM (n = 3 per group). \*##P < 0.001, Sham vs. tMCAO;  $^{AAA}P < 0.001$ , tMCAO+Rp-S (20) vs. tMCAO; \* $^*P < 0.05$ , tMCAO+C-Rp-NPs (0.001) vs. tMCAO; \*\*\*P < 0.001, tMCAO+C-Rp-NPs (0.01) vs. tMCAO and \*\*\*P < 0.001, tMCAO+C-Rp-NPs (0.02) vs. tMCAO (one-way ANOVA with Tukey's multiple comparisons test).



**Fig. 7.** Administration of C-Rp-NPs down regulates the expression of (A) TNF-α, (B) IL-1β and up regulates the (C) dopamine levels in ischemic rats. Data are represented as means  $\pm$  SEM (n = 3 per group). \*\*##P < 0.001, Sham vs. tMCAO;  $^{A\Delta\Delta}P < 0.001$ , tMCAO+Rp-S (20) vs. tMCAO;  $^{ns}P$  = not significant; \*P < 0.05; \*\*\*P < 0.001, tMCAO+C-Rp-NPs (0.001) vs. tMCAO; \*P < 0.001; \*\*\*P < 0.001, tMCAO+C-Rp-NPs (0.01) vs. tMCAO and \*\*\*P < 0.001, tMCAO+C-Rp-NPs (0.02) vs. tMCAO (one-way ANOVA with Tukey's multiple comparisons test).

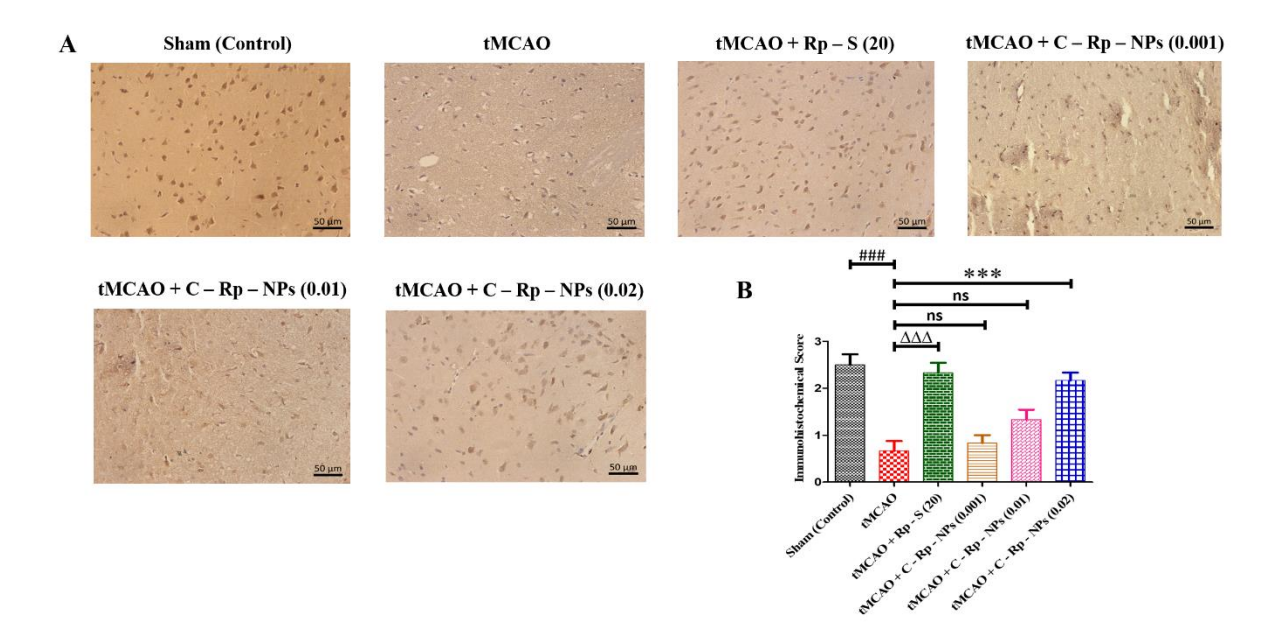


**Fig. 8.** The impact of C-Rp-NPs on D2R expression in the cortical area of ischemic rats. (A) Typical photomicrographs of immunohistochemical staining. (B) Quantitation of immunohistochemistry staining for D2R expression. Data are represented as means  $\pm$  SEM (n = 3 per group). \*##P < 0.001, Sham vs. tMCAO;  $^{\Delta\Delta\Delta}P < 0.001$ , tMCAO+Rp-S (20) vs. tMCAO;  $^{ns}P$  = not significant, tMCAO+C-Rp-NPs (0.001) vs. tMCAO;  $^{ns}P$  = not significant, tMCAO+C-Rp-NPs (0.01) vs. tMCAO and \*\*\*P < 0.001, tMCAO+C-Rp-NPs (0.02) vs. tMCAO (one-way ANOVA with Tukey's multiple comparisons test).

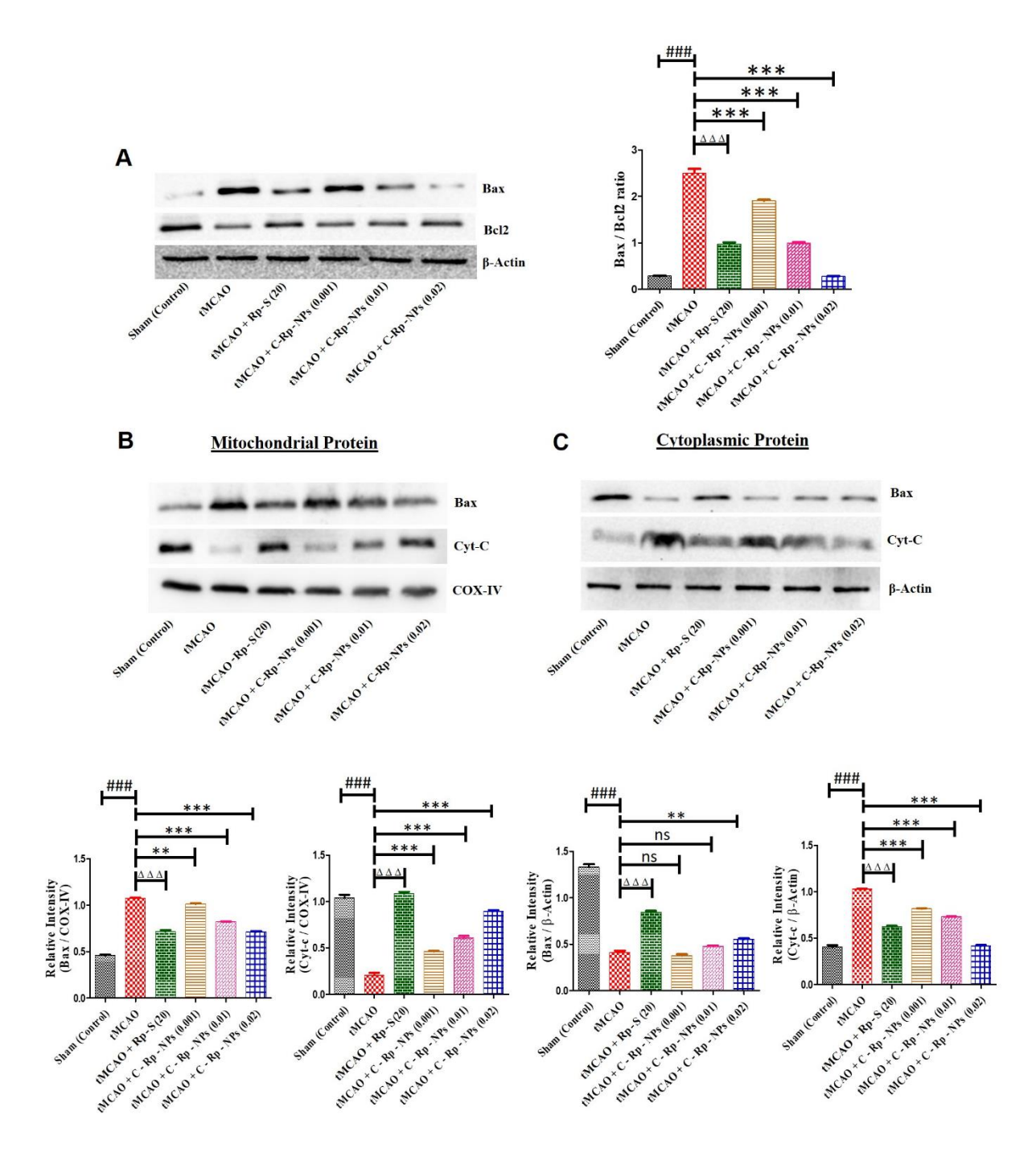


**Fig. 9.** Administration of C-Rp-NPs lowers the Bax/Bcl2 ratio and deters the release of cyt-c as well as translocation of Bax. (A-C) Typical immunoblot intensity indicating (A) Bax/Bcl2 ratio, (B) mitochondrial, and (C) cytosolic Bax and cyt-c. The relative optical intensity of the targeted protein bands were normalized to β-actin and COX-IV. Data are represented as means  $\pm$  SEM (n = 3 per group). \*\*#\*P < 0.001, Sham vs. tMCAO;  $^{\Delta\Delta\Delta}P < 0.001$ , tMCAO+Rp-S (20) vs. tMCAO;  $^{ns}P =$  not significant, \*\*P < 0.001; \*\*\*P < 0.001, tMCAO+C-Rp-NPs (0.001) vs. tMCAO;  $^{ns}P =$  not significant; \*\*\*P < 0.001, tMCAO+C-Rp-NPs (0.01) vs. tMCAO and \*\*P < 0.01; \*\*\*\*P < 0.001, tMCAO+C-Rp-NPs (0.02) vs. tMCAO (one-way ANOVA with Tukey's multiple comparisons test).

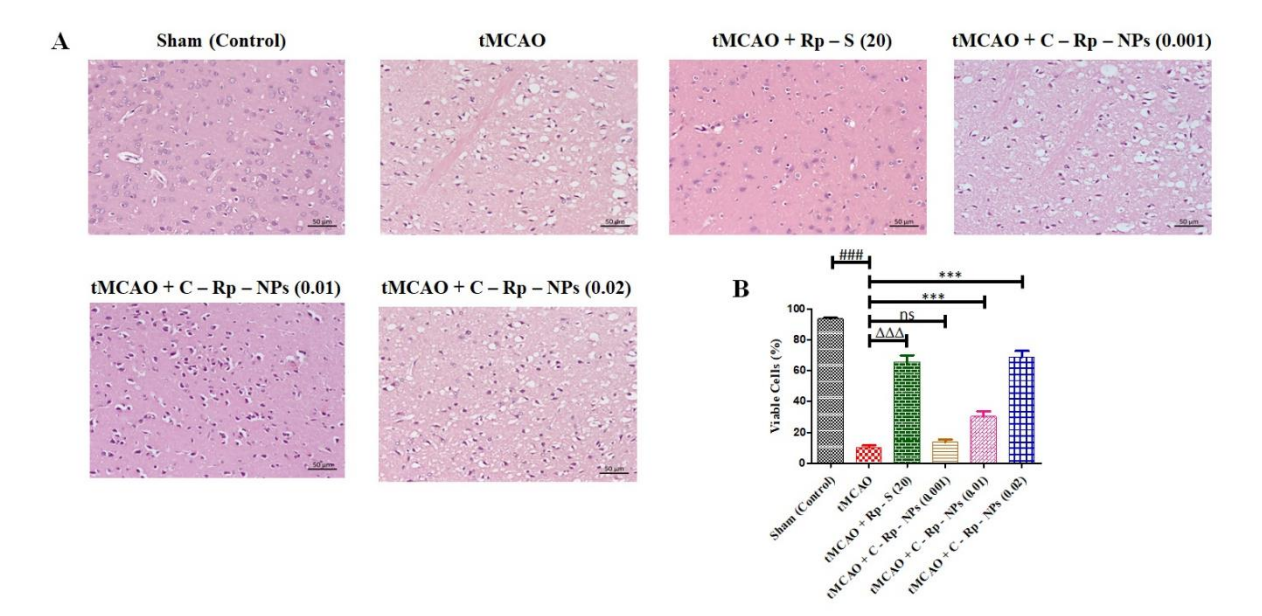


**Fig. 10.** Administration of C-Rp-NPs inhibits neuronal death in ischemic rats. (A) H and E staining of the cortex region. (B) Quantitation of neuronal injury. Data are represented as means  $\pm$  SEM (n = 3 per group). \*\*#\*P < 0.001, Sham vs. tMCAO;  $^{\Delta\Delta\Delta}P < 0.001$ , tMCAO+Rp-S (20) vs. tMCAO;  $^{ns}P$  = not significant, tMCAO+C-Rp-NPs (0.001) vs. tMCAO; \*\*\*P < 0.001, tMCAO+C-Rp-NPs (0.01) vs. tMCAO and \*\*\*P < 0.001, tMCAO+C-Rp-NPs (0.02) vs. tMCAO (one-way ANOVA with Tukey's multiple comparisons test).

 $TABLE\ 1.\ In\ vitro\ cytotoxicity\ assessment\ of\ Rp-S,\ HSA-NPs,\ Rp-NPs,\ and\ C-Rp-NPs\ on\ Neuro-2a\ cell\ lines\ through\ MTT\ assay.$ 

Formulations	Cell Viability (%)±S.D.				
	5 μg/mL	10 μg/mL	15 μg/mL	20 μg/mL	25 μg/mL
Rp-S	89.58±0.011	87.42±0.009	85.23±0.01	80.59±0.005	80.42±0.006
<b>HSA-NPs</b>	100.23±0.051	96.82±0.046	92.99±0.051	90.63±0.071	$87.52\pm0.084$
Rp-NPs	99.16±0.026	97.08±0.006	96.40±0.07	89.58±0.035	86.66±0.017
C-Rp-NPs	99.58±0.015	97.07±0.006	92.40±0.03	90.23±0.02	86.66±0.021

TABLE 2. Plasma and brain distribution profile of Rp-S, Rp-NPs, and C-Rp-NPs (i.p.) in rats.

Formulations	Brain	3 h	6 h	9 h
	Homogenate/Plasma	$(ng/mL)\pm S.D.$	$(ng/mL)\pm S.D.$	$(ng/mL)\pm S.D.$
Rp-S	Plasma	59.2±2.46	11.91±0.59	8.48±0.34
	Brain Homogenate	24.45±0.92	$6.34 \pm 0.22$	4.14±0.21
Rp-NPs	Plasma	254.6±11.52	57.6±2.14	12.5±0.48
	Brain Homogenate	35.71±1.75	449.57±18.62	22.89±0.63
C-Rp-NPs	Plasma	540.69±22.36	159.2±8.15	23.73±1.19
	Brain Homogenate	46.7±3.53	2141.97±77.29	31.64±2.88

## **GRAPHICAL ABSTRACT:**

